Novel trivalent europium β-diketonate complexes with N-(pyridine-2-yl)amides and N-(pyrimidine-2-yl)amides as ancillary ligands: Photophysical properties and theoretical structural modeling

Geórgia B.V. Lima, Jacqueline C. Bueno, Amauri F. da Silva, Albano N. Carneiro Neto, Renaldo T. Moura, Ercules E.S. Teotonio, Oscar L. Malta, Wagner M. Faustino

PII: S0022-2313(19)31445-0

DOI: https://doi.org/10.1016/j.jlumin.2019.116884

Reference: LUMIN 116884

To appear in: *Journal of Luminescence*

Received Date: 22 July 2019

Revised Date: 5 November 2019

Accepted Date: 6 November 2019

Please cite this article as: Geó.B.V. Lima, J.C. Bueno, A.F. da Silva, A.N. Carneiro Neto, R.T. Moura, E.E.S. Teotonio, O.L. Malta, W.M. Faustino, Novel trivalent europium β-diketonate complexes with N-(pyridine-2-yl)amides and N-(pyrimidine-2-yl)amides as ancillary ligands: Photophysical properties and theoretical structural modeling, *Journal of Luminescence* (2019), doi: https://doi.org/10.1016/j.jlumin.2019.116884.

Novel trivalent europium *β*-diketonate complexes with N-(pyridine-2-yl)amides and N-(pyrimidine-2-yl)amides as ancillary ligands: photophysical properties and theoretical structural modeling

Geórgia B. V. Lima[1], Jacqueline C. Bueno[1], Amauri F. da Silva[1], Albano N. Carneiro Neto[2], Renaldo T. Moura Jr.[3], Ercules E. S. Teotonio[1], Oscar L. Malta[4], Wagner M. Faustino[1]

[1] *Department of Chemistry, Federal University of Paraíba, João Pessoa, Brazil*

[2] *Physics Department and CICECO – Aveiro Institute of Materials, University of Aveiro, Aveiro, Portugal*

[3] *Department of Chemistry and Physics, Federal University of Paraíba, Areia, Brazil*

[4] *Department of Fundamental Chemistry, Federal University of Pernambuco, Recife, Brazil*

Abstract

Eighteen new Eu^{3+} complexes and their Gd^{3+} analogs with 1,3-diketonate as main ligands and N-(pyridine-2-yl)amides or N-(pyrimidine-2-yl)amides as ancillary ligands were synthesized. The replacement of water molecules by those amides in the Eu^{3+} complexes increase the intrinsic quantum yields of luminescence, making them comparable or even more efficient than Eu^{3+} complexes with standard ancillary ligands such as 2,2'-bipyridine. The luminescence spectra of Gd^{3+} complexes in comparison with the Eu^{3+} ones show that efficient ligand-to-metal intramolecular energy transfer processes take place. In most cases the experimental Judd-Ofelt intensity parameters (Ω_2 and Ω_4) for the Eu^{3+} complexes show variations as a function of the temperature (77 and 300 K) that overall apparently does not follow clearly any trend. For this reason, geometric variations (on the azimuthal angle ϕ and ancillary ligands distances) were carried out in the coordination polyhedron for simulating thermally induced structural changes. It has been observed that, in this way, the Ω_2 and Ω_4 can be satisfactorily reproduced by *in silico* experiments. It was concluded that, at low-temperature, the ancillary ligands become closer to the Eu^{3+} ion and the angular variations affect more Ω_2 than Ω_4, in agreement to the theoretical calculations. The use of N-(pyridine-2-yl)amides or N-(pyrimidine-2-yl)amides as ancillary ligands in Eu^{3+} 1,3-diketonates looks to be a good strategy for obtaining highly luminescent complexes.

Keywords: Europium, β-diketonates, N-(pyridine-2-yl)amides, N-(pyrimidine-2-yl)amides, intensity parameters, photoluminescence

1. Introduction

The β-diketonates class of ligands is one of the most studied in complexes with Ln^{3+} ions. This is due to its chemical stability, ease of preparation and noticeable emission properties due to the energy transfer (ET) efficiency of these ligands to the Eu^{3+} ion [1–11]. These ligands can act as bidentate by their delocalized charge, forming six-member rings. The Eu^{3+} ions, when coordinated with β-diketonate ligands, are able to provide complexes with high overall emission quantum yields, above 70% [12–17]. This is due to the efficient ligand → Ln^{3+} intramolecular energy transfer, which is largely dependent on the energy difference between the donor and the acceptor states. In order to achieve a more operative intramolecular energy transfer process, the donor state must be above the acceptor state for minimizing the energy back-transfer process [18,19]. A wide variety of Eu^{3+} complexes based on β-diketonate ligands, associated with neutral ligands, are used in light-emitting devices [15] due to its high quantum yield, that can be close to 85% [16] in fluorinated carbazole substituted β-diketonates. Also, novel studies on 2,2':6,6''-terpyridine acting as ancillary ligands reported impressive enhancement in quantum yield (from 31 to 75%) and $^5D_0$ lifetime values (from 0.51 to 1.04 ms) [17]. Besides, incorporations of these compounds onto oxidized multi-walled carbon nanotubes are been used to improve its thermal, photochemical and mechanical stabilities [17].

The lanthanides tris-β-diketonates complexes are part of a highly exploited class of compounds [12,13,20–22]. It can be associated with one, two or three additional neutral ancillary ligands (Lewis bases) in addition to the three β-diketones, depending in general on steric factors, due to the tendency of the Ln^{3+} ion to expand its sphere of coordination, reaching coordination numbers of seven, eight and nine. The most commonly used ancillary ligands are pyridine (PY), bipyridine (BIPY), terpyridine (TERPY) and phenanthroline (PHEN) [23–27]. In the specific case of this work, ligands derived from 2-aminopyridine, 2-aminopyrimidine, and bipyridine were used.

Nitrogen atoms in heterocyclic rings are known to have lone pair electrons to form coordination bonds with empty orbitals of metal ions. In this sense, aromatic PY ligands are suitable candidates to become sensitizing agents to increase the luminescence of the lanthanide ion, due to the ability to bind strongly to these ions and the strong UV absorption [23,28–30].

The combination of three β-diketonates (3-benzoyl-1,1,1-trifluoroacetonate (BTFA), dibenzoylmethanate (DBM) and 2-thenoyltrifluoroacetonate (TTA)) and six ancillary ligands

(N-(pyridine-2-yl)acetamide (NA2AP), N-(pyridine-2-yl)trifluoroacetamide (NTF2AP), N-(pyridine-2-yl)benzamide (NB2AP), N-(pyrimidine-2-yl)acetamide (NA2APM), N-(pyrimidine-2-yl)trifluoroacetamide (NTF2APM) and N-(pyrimidine-2-yl)benzamide (NB2APM)), allowed to obtain 18 new Eu^{3+} based-complexes. The photophysical properties were compared with similar Eu^{3+}-β-diketonate complexes containing either water or BIPY as ancillary ligands which are well-known complexes [27,31–36]. Among these photophysical properties are the intensity parameters Ω_λ.

In this work, we have determined the 4*f*-4*f* intensity parameters (Ω_λ), both experimentally and theoretically, for 18 new complexes. The decay lifetime (τ) of the emitting level $^5D_0$, the radiative and non-radiative spontaneous coefficients (A_{rad} and A_{nrad}, respectively) and the intrinsic quantum yield (Q_{Ln}^{Ln}) were also experimentally determined for both temperatures. Different methodologies can be used to include temperature effects in the theoretical descriptions of lanthanide based-systems [37–42]. In the present case, temperature variations induce structural changes which, consequently, affects the Ω_λ intensity parameters as well as the other photophysical properties (τ, A_{rad}, A_{nrad} and Q_{Ln}^{Ln}). At the present stage, no apparent overall trend in these experimental photophysical properties was observed. This was corroborated by the theoretical calculations, and it is an issue that deserves future more detailed investigation. It is important to comment that this work does not aim a search for new materials with highly efficient properties. Instead, the subject of this work is to analyze the photophysical dependence with the system composition (main and ancillary ligands) and temperature (77 and 300 K).

2. Methodology

2.1. Reagents

Lanthanide oxides (Eu_2O_3 and Gd_2O_3), 2-aminopyridine, 2-aminopyrimidine, concentrated hydrochloric acid, acetic anhydride, acetic acid, pyridine, sodium bicarbonate, acetone, 4,4,4-trifluoro-1-phenyl-1,3-butanedione (HBTFA), dibenzoylmethane (HDBM), thenoyltrifluoroacetone (HTTA) and bipyridine (BIPY) were purchased from Aldrich and used without any previous treatment. Lanthanide(III) chloride hexahydrated ($LnCl_3{\cdot}6H_2O$) was prepared from its respective oxide by salts by reaction with concentrated HCl solution until total decomposition of the solid and final pH close to 6.

2.2. Syntheses of the amide ligands

2.2.1. N-(pyridine-2-yl)acetamide (NA2AP) and N-(pyrimidine-2-yl)acetamide (NA2APM)

The ligand NA2AP was synthesized according to the literature [43], by refluxing equimolar amounts of 2-aminopyridine and acetic anhydride for 2 h. The ligand NA2APM was synthesized according to the same procedure as for NA2AP, but using 2-aminopyrimidine instead of 2-aminopyridine and using three drops of concentrated sulfuric acid as the catalyst. **NA2AP:** m.p. 59-64 °C (lit 60-62 °C [43]); IR (KBr) ν(N-H) 3184, ν(C=O) 1691, ν(C=N) 1535, ν(C=C) 1440, δ(C-N) 625. **NA2APM:** m.p. 143-146 °C; IR (KBr) ν(N-H) 3146, ν(C=O) 1678, ν(C=N) 1522, ν(C=C) 1580, δ(C-N) 642.

2.2.2. N-(pyridine-2-yl)trifluoroacetamide (NTF2AP) and (pyrimidine-2-yl)trifluoroacetamide (NTF2APM)

Into a round bottom flask were added 3.00 g (31.9 mmol) of 2-aminopyridine, 20 mL of chloroform and 2.54 mL (31.9 mmol) of pyridine. The system was left in an ice bath and magnetic stirring until complete solubilization of the 2-aminopyridine. Subsequently, 5.33 mL (38.3 mmol) of trifluoroacetic anhydride was added slowly. The reaction mixture remained under stirring for 30 minutes. The end of the reaction was evidenced by thin-layer chromatography using hexane and ethyl acetate (1:1) as the eluent. The product was isolated by liquid-liquid extraction adding 200 mL of distilled water in the reaction system. The organic phase of extraction was treated with sodium sulfate (Na_2SO_4), filtered and rotoevaporated to give the product as a yellowish oil. The oil was solubilized in diisopropyl ether and cooled in the refrigerator for 24 hours to give a yellowish solid. Finally, the resulting solid was recrystallized from a hexane-chloroform mixture to give a white powder (1.02 g, 33.9%). The ligand NTF2APM was synthesized according to the same procedure as described for NTF2AP, but using 2-aminopyrimidine instead of 2-aminopyridine. **NTF2AP:** m.p. 73-76 °C; IR (KBr) ν(N-H) 3086, ν(C=O) 1693, ν(C=N) 1547, ν(C=C) 1437, δ(C-N) 554. **NTF2APM:** m.p. 145-148 °C; IR (KBr) ν(N-H) 3093, ν(C=O) 1703, ν(C=N) 1549, ν(C=C) 1489, ν(C-N) 1364, δ(C-N) 579.

2.2.3 N-(pyridine-2-yl)benzamide (NB2AP)

Initially, 2 g of 2-aminopyridine (0.0212 mol) was dissolved in 30 ml of chloroform in a round bottom flask. Then, 1.5 mL of benzoyl chloride (0.0106 mol) was added slowly. The system was kept under stirring on an ice bath for 30 minutes. The reaction was monitored by thin-layer chromatography using a hexane/ethyl acetate (1:1) as eluent. Subsequently, 100

mL of a dilute sodium carbonate solution was added to the reaction, separating the product by liquid/liquid extraction. The organic phase was treated with Na_2SO_4, filtered and dried under reduced pressure, to obtain a product as a pale yellow solid. Finally, the resulting solid was recrystallized in a hot hexane/ethanol mixture to give crystals in the form of needles. **NB2AP:** m.p. 79–80°C (lit 81–83°C [44]); IR (KBr) ν(N-H) 3018, ν(C=O) 1672, ν(C=N) 1577, ν(C=C) 1528, δ(C-N) 1306, δ(C-N) 602.

2.2.4 N-(pyrimidine-2-yl)benzamide (NB2APM)

A mass of 5 g of 2-aminopyrimidine (0.03161 mol) was dissolved in 40 ml of a 10% (w/v) NaOH solution in a 250 mL round bottom flask. The solution was refluxed under stirring, and then 4.4 g of benzoyl chloride (0.03160 mol, 3.70 mL) was slowly added to the system. The reaction occurred quickly and the color change from colorless to yellow. The end of the reaction was monitored by thin-layer chromatography using a hexane/ethyl acetate (1:1) as eluent. After 30 minutes, the system was cooled to room temperature, forming a yellow solid. The product was filtered under reduced pressure, and the solid was washed six times with a 10% NaOH solution. The solid obtained was recrystallized to a low-temperature ethanol/hexane mixture (approximately -4°C), resulting in yellowish crystals. **NB2APM:** m.p. 167-170°C; IR (KBr) ν(N-H) 3053, ν(C=O) 1713, ν(C=N) 1576, ν(C=C) 1543, δ(C-N) 1317, δ(C-N) 615.

2.3 Syntheses of the complexes

The hydrated complexes $[Ln(\beta\text{-dik})_3(H_2O)_x]$ (where β-dik = BTFA, DBM and TTA; Ln = Eu^{3+} and Gd^{3+}; x = 1 or 2), where synthesized as described [45]. The complexes with amide ligands were synthesized by the reaction between the $[Ln(\beta\text{-dik})_3(H_2O)_x]$ complex and NA2AP, NA2APM, NTF2AP, NTF2APM, NB2AP, NB2APM, and BIPY dissolved in acetone (molar ratio between complex with aquo ligands and amide ligands of 1:1). The mixture was stirred and evaporated at room temperature. The solid products were washed with water to remove excess amide ligand. The synthesis is illustrated in Scheme 1.

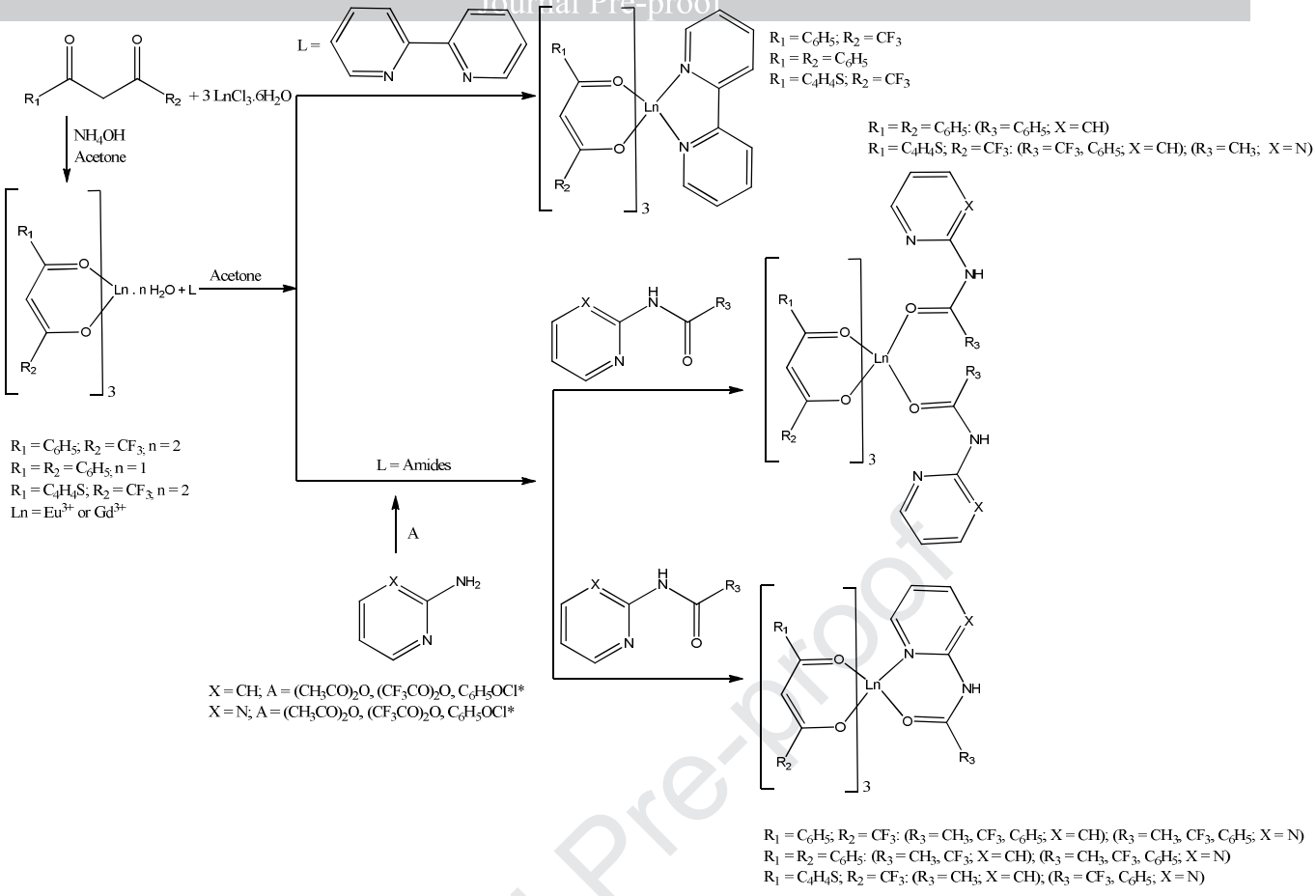

Scheme 1. Synthetic route for $[Ln(\beta\text{-dik})_3(L)_x]$ complexes (Ln = Eu^{3+} and Gd^{3+}; β-dik = BTFA, DBM and TTA; L = NA2AP, NA2APM, NTF2AP, NTF2APM, NB2AP and NB2APM; x = 1 or 2).

2.4. Apparatus

The carbon and hydrogen content was determined by the usual microanalytical procedures using an elemental analyzer model CHN 2400 (Perkin-Elmer, USA) while the Eu^{3+} content was obtained by complexometric titration with EDTA using xylenol orange as indicator. NMR studies of ligands were carried out on a Varian Spectrometer 400 MHz for ^{1}H and ^{13}C (Supporting Information).

The infrared spectra of the samples were used to provide information about the coordination nature of NA2AP, NA2APM, NTF2AP, NTF2APM, NB2AP, NB2APM and BIPY ligands to the Ln^{3+} ions. These spectra were recorded in the range from 4000 to 400 cm^{-1} in KBr pellets, using a Shimadzu FTIR spectrophotometer model IRPRESTIGE-21.

The thermogravimetric curves of the complexes were obtained using a simultaneous thermal analyzer Shimadzu DTG-60H. To perform the analysis, approximately 5 mg of the

complexes were placed in a sample holder and heated at a rate of 10 °C·min^{-1}, with a flow rate of 30 mL·min^{-1}, in the range of 30-900°C in a synthetic air atmosphere.

Steady-state excitation and emission spectra at room (~298 K) and liquid nitrogen (77 K) temperatures were recorded at an angle of 22.51 (front face) with a spectrofluorimeter (FLUOROLOG 3) with double grating 0.22 m monochromator (SPEX 1680), and a 450 W Xenon lamp as the excitation source. All spectra were recorded using a detector mode correction. The luminescence decay curves of the emitting levels were measured using a phosphorimeter SPEX 1934D accessory coupled to the spectrofluorometer.

2.5 Experimental and theoretical photophysical properties

The radiative spontaneous emission rate $A_{J\to J'}$ from the emitting J level to a lower J' level is given by [18,46–48]:

$$A_{J\to J'} = \frac{4e^2\omega^3}{3\hbar c^3}\left[\frac{n(n^2+2)^2}{9}S_{ED} + n^3 S_{MD}\right] \quad (1)$$

where e is the elementary charge, ω is the angular frequency of the transition, $\hbar$ is the Planck's constant over 2π (~1.05×10^{-27} erg·s), n is the index of refraction of the medium, c is the speed of light, and, S_{ED} and S_{MD} are the electric dipole and magnetic dipole strengths, respectively (in units of e^2).

Each transition $A_{J\to J'}$ can be calculated taking the $^5D_0\to{}^7F_1$ transition (almost 100% governed by the magnetic dipole mechanism) as a reference, $S_{MD} = 9.6\times10^{-6}$ D^2 for this transition, while $S_{MD} = 0$ for all other transitions. S_{ED} is given by Eq. (2):

$$S_{ED} = \frac{1}{2J+1}\sum_{\lambda=2,4,6}\Omega_\lambda\langle\psi J\|U^{(\lambda)}\|\psi' J'\rangle^2 \quad (2)$$

where $2J+1$ is the degeneracy of the emitting state (equal to 1 for the $^5D_0$ of the Eu^{3+} state).

In the case of Eu^{3+} complexes, the Eq. (2) can be used without the summation over λ since the intensity of each $^5D_0\to{}^7F_\lambda$ (λ = 2, 4, 6) transition is determined only by a single Ω_λ intensity parameter. In addition, the experimental Ω_6 is not determined since the $^5D_0\to{}^7F_6$ transition is rarely observed.

For lifetime measurements on Eu^{3+} compounds, typically a microsecond flash lamp is used. The time-dependent intensity is measured following the excitation pulse:

$$I(t) = I(0)e^{-\frac{t}{\tau_{tot}}} \quad (3)$$

where $I(t)$ is the intensity at time t, $I(0)$ is the intensity at time $t = 0$ s, and τ_{tot} is the total emission lifetime.

The rate of relaxation of an excited state J is governed by the combination of the probabilities for radiative (A_{rad}) and non-radiative decay processes (A_{nrad}). The lifetime, non-radiative and radiative rates are related by Eq. (4):

$$A_{tot} = \frac{1}{\tau_{tot}} = \sum_{J'} A_{rad}(J \to J') + \sum_{J'} A_{nrad}(J \to J') \quad (4)$$

where the summations are for transitions over all J' states. A_{rad} rates were obtained in terms of the areas ($S_{0\to J'}$) under the emission spectrum by Eq. (5) [49]:

$$A_{0\to J} = \left(\frac{S_{0\to J'}}{S_{0\to 1}}\right) A_{0\to 1} \quad (5)$$

where $A_{0\to 1} \cong 50$ s^{-1} for $n = 1.5$ [47]. Knowing the $A_{0\to J}$ ($J = \lambda$), the experimental Ω_λ can be determined by:

$$\Omega_\lambda = \frac{3\hbar c^3 A_{0\to\lambda}}{4e^2\omega^3\chi\langle {}^7F_\lambda \| U^{(\lambda)} \| {}^5D_0\rangle^2} \quad (6)$$

where $\chi = n(n^2+2)^2/9$ is the Lorentz local field correction and $\langle {}^7F_\lambda \| U^{(\lambda)} \| {}^5D_0\rangle^2$ are the square reduced matrix elements with values 0.0032 and 0.0023 for $\lambda = 2$ and 4, respectively [50].

In this work, the theoretical intensity parameters will be indicated using the superscript *theo* (Ω_λ^{theo}). From then, information about the chemical environment around the Ln^{3+} can be extracted. These parameters contain two main contributions: the Forced Electric Dipole (FED) [51,52] and Dynamic Coupling (DC) mechanisms [18,53–55]. The Ω_λ^{theo}, according to the treatment in Refs. [56–58], can be calculated using Eqs. (7)–(9):

$$\Omega_\lambda^{theo} = (2\lambda+1)\sum_{t,p}\frac{\left|B_{\lambda tp}\right|^2}{2t+1} \quad , \quad B_{\lambda tp} = B_{\lambda tp}^{FED} + B_{\lambda tp}^{DC} \quad (7)$$

where,

$$\mathrm{B}_{\lambda tp}^{FED} = \frac{2}{\Delta E}\langle r^{t+1}\rangle \Theta(t,\lambda)\left(\frac{4\pi}{2t+1}\right)^{1/2}\left(\sum_j e^2 \rho_j g_j (2\beta_j)^{t+1}\frac{Y_{p,j}^{t*}}{R_j^{t+1}}\right) \tag{8}$$

$$B_{\lambda tp}^{DC} = -\left[\frac{(\lambda+1)(2\lambda+3)}{(2\lambda+1)}\right]^{\frac{1}{2}}\langle r^{\lambda}\rangle\langle f\|C^{(\lambda)}\|f\rangle \times \\ \times\left(\frac{4\pi}{2t+1}\right)^{\frac{1}{2}}\left(\sum_j\left[(2\beta_j)^{t+1}\alpha_{OP,j}+\alpha_j'\right]\frac{Y_{p,j}^{t*}}{R_j^{t+1}}\right)\delta_{t,\lambda+1} \tag{9}$$

Eqs. (8) and (9) corresponding to the FED and DC mechanism, respectively. Here a brief explanation about the quantities shown in the above equations is given. More details on all these expressions can be found in Refs. [56–58] and references therein.

In the FED mechanism (Eq. (8)), the ΔE comes from an extension of the average energy denominator method by Bebb and Gold [59,60], the $\Theta(t,\lambda)$ are factors that involves operations on the reduced matrix elements of $f \rightarrow g$ and $f \rightarrow d$ transitions of the lanthanide ion, the $g's$ are the charge factors associated with the overlap integrals (ρ) between the ligating atom (or ion) and the Ln^{3+} ion. $Y_{p,j}^{t*}$ are spherical harmonics. The molecular symmetry is taken into account by the sum over j.

According to the BOM model [61,62], the polarizabilities α_{OP} (Eq. (10)) and α' are associated to the chemical bonding and the influence of the ligand environment near to the Ln^{3+} ion, respectively [61]. The g factors, in Eq. (8), are also associated to the chemical bond and can be interpreted as the capacity of atomic species to donate electronic density to the bond formation [63], it can be calculated by Eq. (11):

$$\alpha_{OP} = \frac{e^2\rho^2R^2}{2\Delta\varepsilon} \tag{10}$$

$$g = R\sqrt{\frac{k}{2\Delta\varepsilon}} \tag{11}$$

where the R is the equilibrium distance, k is the force constant and $\Delta\varepsilon$ is the first excitation energy, all these quantities are associated with the Ln^{3+}–X (X = ligating atom or ion) chemical bond.

The JOYSpectra program, developed by our group, was used for the calculation of Ω_{λ}^{theo}. This program can perform some analysis changing the symmetry, chemical environment, etc. It can be accessed through the website www.cca.ufpb.br/gpqtc/joyspectra.

2.6 *In silico* experiments

All molecular structures of the complexes were fully optimized. The harmonic force constants (k) were calculated numerically using a five-point finite difference method [64] and the dipolar polarizabilities were calculated using finite-field approach within the Gaussian 09 [65] and MOPAC [66] programs. The molecular orbitals in the isolated ligands were localized using the Pipek-Mezey procedure [67] and decomposition of the total molecular polarizability into contributions from each localized molecular orbital (LMO) for the isolated ligands in the optimized geometry of the complex was performed with the GAMESS program [68]. The geometry optimization calculations were performed at the B3LYP level using the 6-311++G(d,p) basis set for hydrogen, carbon, nitrogen, oxygen, fluorine and sulfur atoms, while the core potential MWB52, which includes 52 electrons in the core, was used with its associated valence basis set for the europium atom [69]. The charge factors were calculated using Sparkle/PM3 [70,71] methodology, where the geometries were pre-optimized and pseudo-diatomic force constants [61] were calculated. The dipolar polarizability and its decomposition into LMO contributions for the ligands were calculated with the B3LYP/aug-cc-pVDZ method. The overlap integrals (ρ) were calculated using the BP86/STO-TZ2P method within the ADF program [72].

3. Results and discussion

3.1. Characterization of the [Ln(β-dik)$_3$(L)$_x$] complexes

3.1.1. Elemental analysis

The Ln amount was estimated by complexometric titration with EDTA, where the compounds were dissolved in acetone using xylenol orange as an indicator. The carbon, hydrogen, and nitrogen quantities were determined by usual microanalytical procedures.

The results, in the **Supporting Information**, show that the calculated and experimental values are close to each other, indicating that the composition of the complexes is consistent to [Ln(BTFA)$_3$(L)] (L = NA2AP, NA2APM, NTF2AP, NTF2APM, NB2AP, NB2APM and BIPY), [Ln(DBM)$_3$(L)] (L = NA2AP, NA2APM, NTF2AP, NTF2APM, NB2APM and BIPY),

$[Ln(TTA)_3(L)]$ (L = NA2AP, NTF2APM, NB2APM and BIPY), $[Ln(DBM)_3(L)_2]$ (L = NB2AP) and $[Ln(TTA)_3(L)_2]$ (L = NA2APM, NTF2AP e NB2AP).

All the complexes studied in this article have coordination numbers equal to eight, with the lanthanide ion bound to eight oxygen and/or nitrogen atoms from the ligands. The trivalent ion is coordinated to three β-diketones and one or two heteroaromatic ligands.

3.1.2. Infrared spectroscopy

Vibrational spectra in the infrared region provide important information about the nature of the carbonyl groups of the β-diketonates and the amide ligands coordinated to the metal ions in the complex. The infrared spectra (Figs. S1–S9) of β-diketones HBTFA, HDBM, and HTTA present strong bands at 1595, 1597 and 1659 cm^{-1} respectively, which is attributed to the ν (C=O) stretching mode. In the lanthanide complexes, this band is significantly shifted to a lower frequency region, evidencing that the metal ion is coordinated through the oxygen atoms [73].

The complexes with aquo ligands exhibit broadband in the region of 3500 to 3300 cm^{-1}, attributed to the stretch ν(O-H) of the water molecules bound to the metal center. Thus, it is expected that in the IR spectra of the complexes with the amide ligands, such a band is not observed proving the substitution of these water molecules by the amide ligands.

The analysis of infrared spectroscopy is in accordance with the proposal that amides (L = NA2AP, NA2APM, NTF2AP, NTF2APM, NB2AP, NB2APM, and BIPY) coordinate in a bidentate mode to the central ion. The free amides containing carbonyl have their stretching bands ν(C=O) attributed around 1690 cm^{-1} [74]. However, these bands are shifted to the lower energy region when these ligands coordinate to the metal center through the carbonyl oxygen. For the coordination of the nitrogen of the pyridyl group, the displacement of the band attributed to the deformation of the ring in the pyridine plane, associated with bands at approximately 605 cm^{-1}, is considered. Thus, when coordination occurs through nitrogen, this band is shifted to regions of higher frequency. In the complexes $[Ln(DBM)_3(NB2AP)_2]$ and $[Ln(TTA)_3(L)_2]$ (L = NA2APM, NTF2AP, and NB2AP) the coordination of the amides to the metal center occurs in a monodentate way through oxygen.

Fig. 1 shows the infrared spectra of the $[Eu(BTFA)_3(NB2AP)]$ and $[Eu(DBM)_3(NB2AP)_2]$ complexes. In the $[Eu(DBM)_3(NB2AP)_2]$ complex, the coordination of the amide to the metal center occurs in a monodentate way through the oxygen, thus allowing the coordination of two amides to the Ln^{3+} ion. For the $[Eu(BTFA)_3(NB2AP)]$ complex the amide was coordinated to the metal in bidentate form because the band corresponding to the stretch

ν(C=O) was displaced to the lower energy region when compared to the NB2AP free ligand. In addition, the band displacement attributed to the deformation of the ring in the plane of the pyridine to the region of higher frequency occurred, demonstrating the coordination through the nitrogen. For the others isolated ligands and Eu^{3+} complexes, the FTIR spectra are shown in Figs. S1-S9.

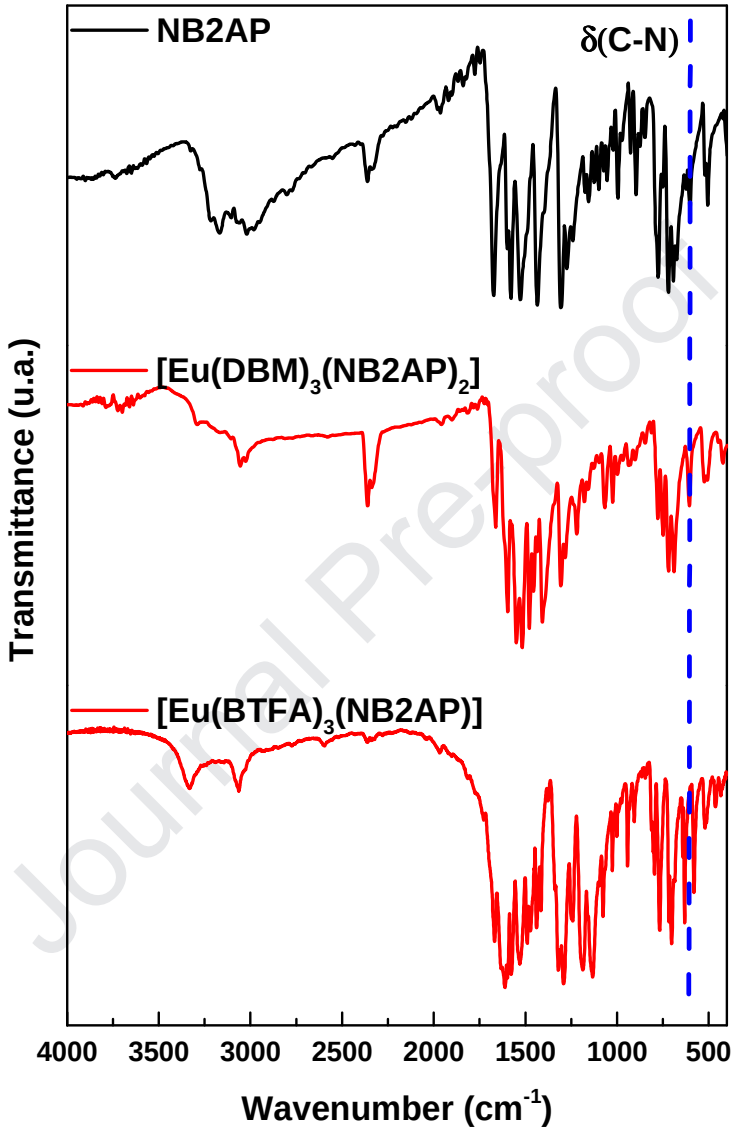

Figure 1. The absorption spectrum in the infrared region for the NB2AP ligand and the $[Eu(DBM)_3(NB2AP)_2]$ and $[Eu(BTFA)_3(NB2AP)]$ complexes.

3.1.3. Thermogravimetric analysis

Thermal analysis TG curves (in the Supporting Information) have been used to characterize the thermal stability of the complexes. The TG curves of the europium complexes with BTFA, DBM and TTA ligands, and amide ligands (NA2AP, NA2APM, NTF2AP, NTF2APM, NB2AP, NB2APM, and BIPY) were recorded in the range of 30 to 900°C under an atmosphere of synthetic air (30 mL·min^{-1}).

It was verified that the TG curves of europium β-diketonate complexes do not present events related to water loss. This result is in agreement with the data of CHN and absorption spectroscopy in the infrared region, evidencing the anhydrous character of the synthesized complexes. In all curves, the most effective mass losses are located mainly in the range of 108 to 435°C, resulting from the elimination of high molecular weight ligands. The loss of mass in these compounds occurs until their more volatile components are eliminated, resulting in residues that may be associated with the Eu_2O_3. Information on the percentage values of mass loss in the thermodecomposition steps, as well as the temperature ranges, are shown in Table S1.

In the complexes with β-diketone BTFA, $[Eu(BTFA)_3(L)]$, the first event, with mass loss of approximately 61%, occurs in the range of 115-350°C and was attributed to the exit of the three ligands BTFA. In complexes with DBM, $[Eu(DBM)_3(L)_x]$, there is a significant loss around 300°C. For the case of TTA compounds, $[Eu(TTA)_3(L)_x]$, the first loss event is approximately 58% of the initial mass.

It is important to note that most of the TTA complexes with amide ligands initiates their thermal decompositions by approximately 130°C, while the BTFA in 115°C and DBM in 110°C complexes, indicating the higher thermal stability of the TTA complexes.

3.2. Photoluminescence investigations

To estimate the excited T_1 states of the ligands in the Eu^{3+} complexes, the phosphorescence spectra of the analogous Gd^{3+} complexes were recorded (Fig. S11). The Gd^{3+} complexes do not present intraconfiguration-4*f* transitions in the visible region. In addition, the ionic rays of the Eu^{3+} and Gd^{3+} ions are very close, in this way the Gd^{3+} complexes can be used as mimics for the Eu^{3+} complexes [73]. In the scope of the present work, the detailed role of the S_1 and T_1 states of the ligands will not be discussed, except for the noticeable fact that the broadband emission in the Gd^{3+} complexes (Fig. S11) do not appear in the case of the emission spectra of the Eu^{3+} complexes (Figs. 3 and 4), indicating efficient ligand-to-metal intramolecular energy transfer. This is an open issue that is the reason for forthcoming work.

Fig. 2 shows the excitation spectra (monitored at the $^5D_0 \rightarrow {}^7F_2$ transition, 612 nm) at the 77 K for the complexes $[Eu(\beta\text{-dik})_3(L)_x]$ (L = H_2O, NA2AP, NA2APM, NTF2AP, NTF2APM, NB2AP, NB2APM and BIPY; x = 1 or 2). Aside from the wide ligands bands, thin bands appear between 450 and 590 nm ($^7F_0 \rightarrow {}^5D_2$ at 465 nm, $^7F_0 \rightarrow {}^5D_1$ at 526 nm and $^7F_0 \rightarrow {}^4G_6$ at 579 nm), all of which originate from 4*f*-4*f* transitions, which can populate the emitting levels of the Eu^{3+}

ion. Also, fine peaks assigned to the intraconfiguration 4*f*-4*f* transitions are overlapped with the ligand bands, these peaks arising from the ground state $^{7}F_{0}$ and following the levels: $^{4}G_{6}$ (~361 nm), $^{5}H_{4}$ (~374 nm) and $^{5}L_{6}$ (~394 nm) [75].

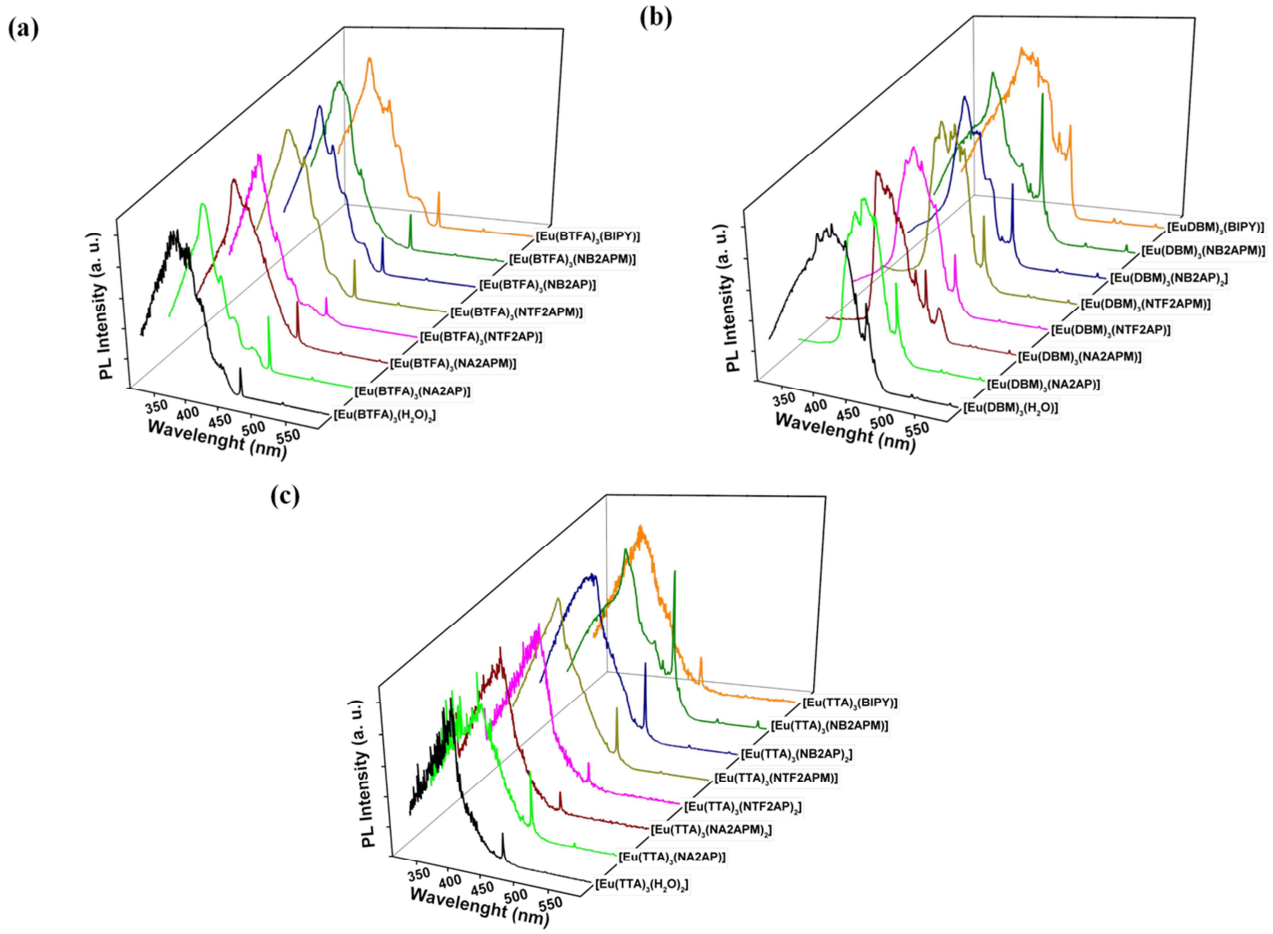

Figure 2. Excitation spectra of the complexes recorded at 77 K, under emission at 612 nm assigned to the $^{5}D_{0} \rightarrow {}^{7}F_{2}$ transition of the Eu^{3+} íon: (a) $[Eu(BTFA)_{3}(L)]$; (b) $[Eu(DBM)_{3}(L)_{x}]$; (c) $[Eu(TTA)_{3}(L)_{x}]$.

The emission spectra were recorded, with excitation monitored at 394 nm ($^{7}F_{0}\rightarrow{}^{5}L_{6}$ transition), at 300 and 77 K (Figs. 3 and 4, respectively) in solid-state samples. These spectra exhibit fine bands assigned to the $^{5}D_{0}\rightarrow{}^{7}F_{J}$ transitions (where J = 0, 1, 2, 3 and 4), with the $^{5}D_{0}\rightarrow{}^{7}F_{2}$ transition being the most intense.

The spectra at both temperatures have different profiles, as can be noted when Figs. 3 and 4 are compared. These differences indicate that the complexes undergo some structural changes influenced by the temperature.

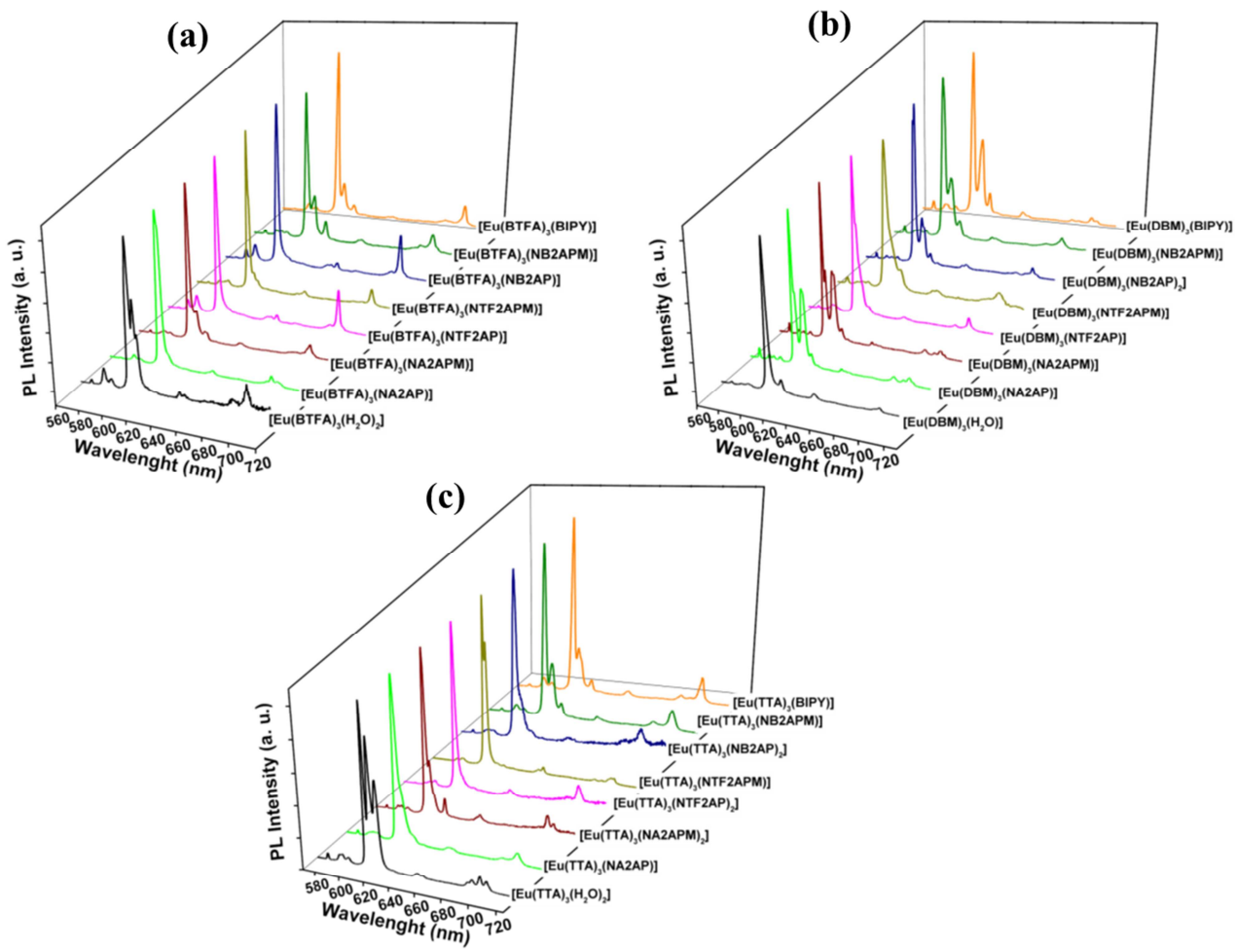

Figure 3. Emission spectra of the complexes [Eu (β-dik)$_3$(L)$_x$] in the range of 570 to 720 nm, recorded at 300 K: (a) [Eu(BTFA)$_3$(L)]; (b) [Eu(DBM)$_3$(L)$_x$]; (c) [Eu(TTA)$_3$(L)$_x$], λ_{exc} = 394 nm.

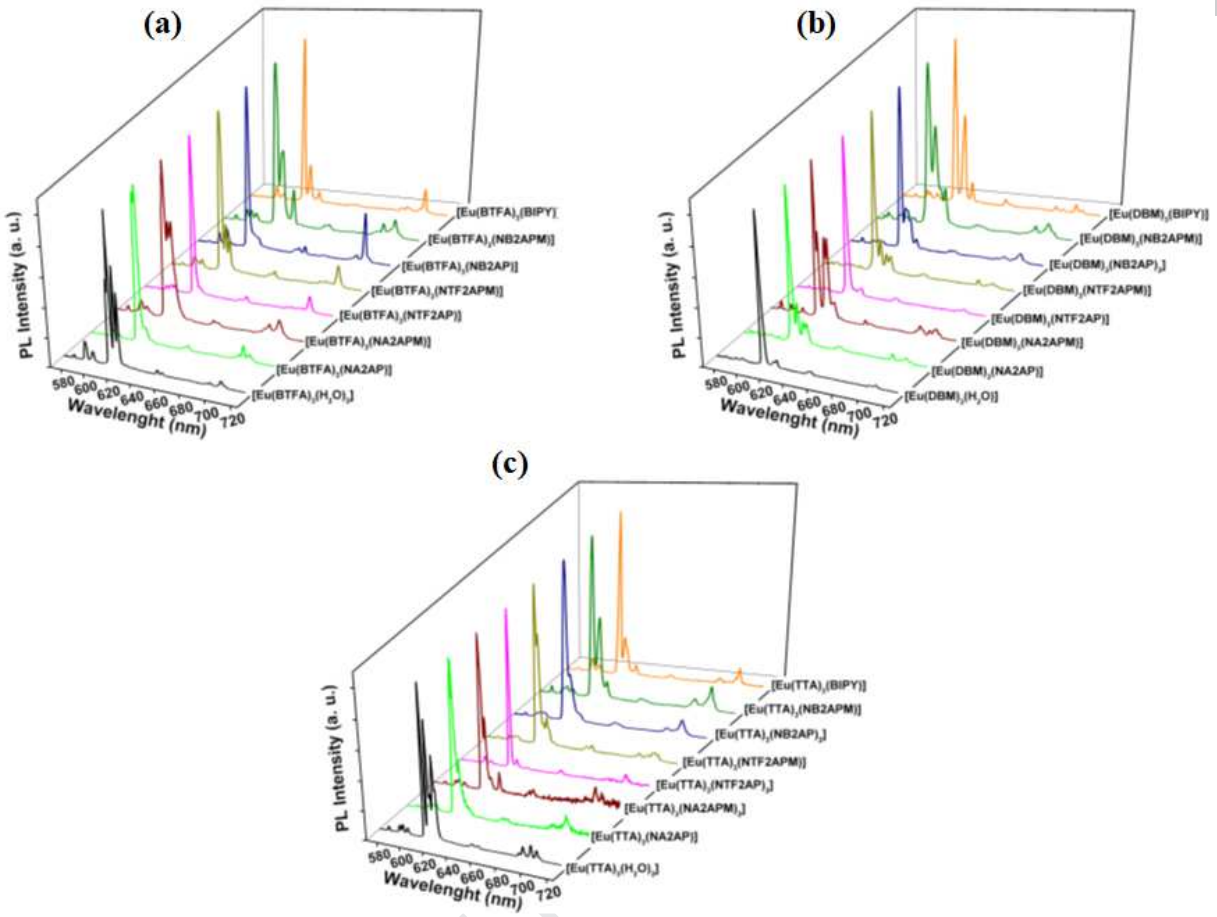

Figure 4. Emission spectra of the complexes [Eu (β-dik)$_3$(L)$_x$] in the range of 570 to 720 nm, recorded at 77 K: (a) [Eu(BTFA)$_3$(L)]; (b) [Eu(DBM)$_3$(L)$_x$]; (c) [Eu(TTA)$_3$(L)$_x$], λ_{exc} = 394 nm.

The $^5D_0 \rightarrow {}^7F_0$ transition is prohibited by forced electric dipole and magnetic dipole mechanisms. Though it may be allowed by symmetry. However, provided it is allowed by symmetry these selection rules on the mechanisms can be relaxed by the electric dipole mechanism due to the ligand field leading to the *J* mixing effect [75]. A single peak of this transition is observed at ~580 nm, suggesting that the Eu^{3+} ion is in a low symmetry chemical environment, classified as one of the symmetries C_{nv}, C_n or C_s [75]. The bands referring to the other intraconfiguration transitions $^5D_0 \rightarrow {}^7F_J$ (J = 1, 2, 3 and 4), show deployments of at most $2J + 1$ components, indicating that the Eu^{3+} ion is in a low symmetry chemical environment. However, the spectra of the [Eu(DBM)$_3$(NA2AP)], [Eu(DBM)$_3$(NA2APM)], [Eu(DBM)$_3$(NTF2AP)] and [Eu(DBM)$_3$(NB2APM)] have two peaks for the $^5D_0 \rightarrow {}^7F_0$ transition, suggesting at least two different chemical environments around the Eu^{3+} ion.

It has been observed that in general, the emission spectra of the hydrated complexes [Eu(β-dik)$_3$(H$_2$O)$_x$] and substituted [Eu(β-dik)$_3$(L)$_x$] exhibit quite different profiles, suggesting the substitution of the water molecules for the amide ligands. Moreover, the substituted

complexes of DBM present a greater number of bands (greater unfolding), when compared to the respective hydrated complexes, suggesting a smaller symmetry in the first ones. In the case of the complexes with BTFA and TTA, the hydrated complexes that present a greater number of bands, suggesting a smaller symmetry for the new compounds obtained. It is also possible to observe in these spectra that the simple change of the auxiliary ligand causes a significant change in the spectral profile, suggesting chemical environments significantly different from the amide ligand exchange.

Fig. 5 shows representative curves for the luminescence decay from the $^5D_0$ state at low temperature. These decay curves were recorded with excitation at 394 nm and emission monitored at 612 nm. The luminescence lifetime (τ_{tot}) were obtained by a monoexponential fitting (Table 1). We have also obtained the luminescence decay curves exciting the complexes at 465nm (Supplementary materials). As it can be seen in Table 1 there is no appreciable differences between excitation at 394 and 465 nm for the new investigated complexes.

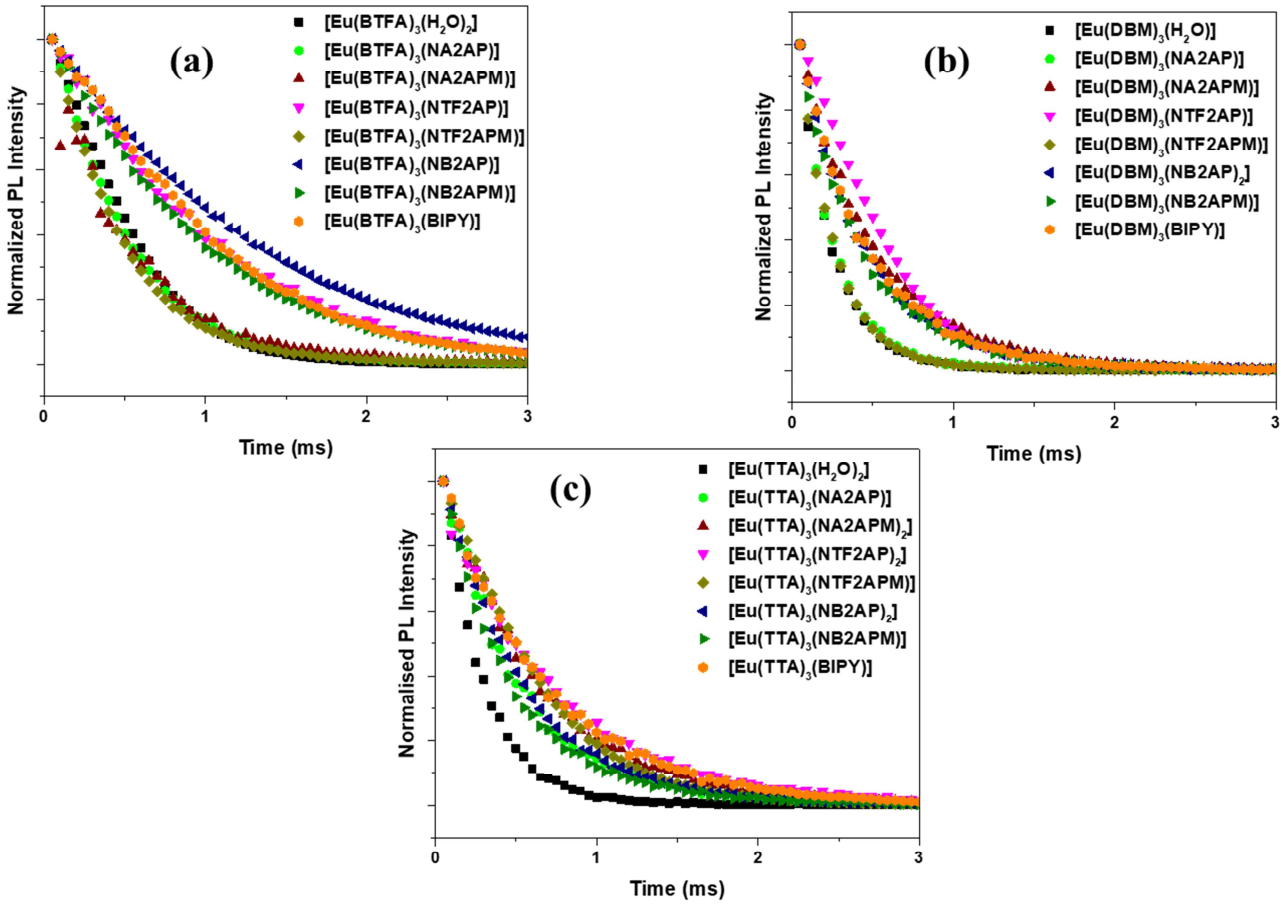

Figure 5. Luminescence decay curves for $[Eu(\beta\text{-dik})_3(L)_x]$ complexes: β-dik = BTFA (a), DBM (b), and TTA (c), λ_{exc} = 394 nm, 77 K.

The intrinsic quantum yield Q_{Ln}^{Ln} is observed for direct excitation in the lanthanide 4*f* levels. If the A_{rad} is known, Q_{Ln}^{Ln} can be calculated from the observed luminescence lifetime:

$$Q_{Ln}^{Ln} = \frac{\tau_{tot}}{\tau_{rad}} = \frac{A_{rad}}{A_{tot}} \quad (12)$$

3.3 Experimental and theoretical photophysical properties

Tables 1 shows the experimental intensity parameters Ω_λ (λ = 2 and 4) for the Eu^{3+} complexes. The values of the intensity parameters Ω_2 are higher for the DBM complexes compared to those of BTFA and TTA at 300 and 77 K. These data indicate that the Eu^{3+} ion in the DBM compounds is in a more polarizable chemical environment than in the complexes with the other β-diketones [73]. This result is corroborated by the theoretical effective ligand polarizabilities, as it will be discussed in **section 3.4**.

The values of A_{rad} shows a small variation between the temperatures. However, the substitution of the water molecules for the amide ligands produce a large difference in this rate. The high values of A_{nrad} for the hydrated complexes indicate that the multiphonon decay of the water molecules, such as ν_s(OH) and ν_{ass}(OH), are the main operational route that depopulates the $^5D_0$ emitting level [76]. The evidence for this mechanism is given by the significant decrease in A_{nrad} values when the water molecules were replaced by the amide ligands. However, for [Eu(BTFA)$_3$(NTF2APM)], [Eu(DBM)$_3$(NA2AP)] and [Eu(DBM)$_3$(NTF2APM)] (entries 5, 10 and 13 in Table 1) complexes at 77 K, the values of A_{nrad} still greater than their respective complexes with aquo ligands. At room temperature, the [Eu(DBM)$_3$(L)$_x$] complexes present a decrease in the A_{rad} values when compared to their respective aquo complexes, except for the [Eu(DBM)$_3$(NA2APM)] and [Eu(DBM)$_3$(NB2AP)$_2$] (entries 11 and 14 in Table 1) complexes.

In general, excluding the above-discussed complexes, it was observed that the substitution of the water molecule by amide ligands resulted in a drastic decrease in A_{nrad} rates. This fact also resulted in an increase of the emission lifetime, and, consequently, an increase in the values of the intrinsic quantum yield.

The complexes [Eu(DBM)$_3$(L)] present coordination mode to the metal center similar to the complex [Eu(DBM)$_3$PX] [4]. The latter presents a lower lifetime than the new complexes of the same class at 300 K, except for the [Eu(DBM)$_3$(NTF2APM)] (entry 13 in Table 1) complex.

Table 1 Experimental intensity parameters (Ω_λ), radiative (A_{rad}) and non-radiative (A_{nrad}) decay rates, emission lifetime and intrinsic quantum yield (Q_{Ln}^{Ln}) of the [Eu(β-dik)$_3$(L)$_x$] compounds, where L = H_2O, NA2AP, NA2APM, NTF2AP, NTF2APM, NB2AP, NB2APM and BIPY; x = 1 or 2.

Entry	Complex	Ω_2 (10^{-20} cm^2)*		Ω_4 (10^{-20} cm^2)*		A_{rad} (s^{-1})*		A_{nrad} (s^{-1})*		$\tau_{465\ nm}$ (ms)		$\tau_{394\ nm}$ (ms)		Q_{Ln}^{Ln} (%)*	
		300 K	77 K	300 K	77 K	300 K	77 K	300 K	77 K	300 K	77 K	300 K	77 K	300 K	77 K
1	**[Eu(BTFA)$_3$(H$_2$O)$_2$]**	14.8	13.9	7.8	1.6	642	507	1840	1551	0.34±0.01	0.35±0.02	0.39±0.02	0.37±0.02	24.7	18.9
2	**[Eu(BTFA)$_3$(NA2AP)]**	30.6	29.7	6.5	8.7	1110	1119	1054	995	0.44±0.01	0.43±0.01	0.52±0.03	0.49±0.03	57.3	54.6
3	**[Eu(BTFA)$_3$(NA2APM)]**	24.9	19.6	11.5	5.6	1020	746	1419	1219	0.36±0.05	0.42±0.04	0.36±0.04	0.42±0.03	36.5	31.2
4	**[Eu(BTFA)$_3$(NTF2AP)]**	9.7	18.2	6.0	7.0	466	740	778	273	0.70±0.05	0.52±0.05	0.73±0.05	0.77±0.11	34.1	57.3
5	**[Eu(BTFA)$_3$(NTF2APM)]**	16.2	16.3	6.1	5.6	666	651	1828	1627	0.42±0.04	0.36±0.02	0.44±0.05	0.42±0.05	29.1	27.2
6	**[Eu(BTFA)$_3$(NB2AP)]**	9.7	11.1	6.0	6.1	464	506	631	293	0.71±0.03	0.49±0.03	0.97±0.09	0.73±0.02	45.1	36.8
7	**[Eu(BTFA)$_3$(NB2APM)]**	17.6	19.1	14.4	6.1	845	738	679	353	0.61±0.01	0.60±0.03	0.71±0.08	0.71±0.09	59.7	52.3
8	**[Eu(BTFA)$_3$(BIPY)]**	20.4	19.0	8.2	7.8	804	750	465	270	0.76±0.01	0.71±0.01	0.85±0.04	0.87±0.11	68.1	65.2
9	**[Eu(DBM)$_3$(H$_2$O)]**	31.6	41.3	4.2	3.1	1124	1415	7804	3280	0.05±0.01	0.20±0.02	0.07±0.01	0.26±0.01	8.2	37.1
10	**[Eu(DBM)$_3$(NA2AP)]**	30.2	33.0	5.7	5.3	1091	1190	3884	3315	0.16±0.04	0.22±0.01	0.31±0.03	0.29±0.02	33.5	34.2
11	**[Eu(DBM)$_3$(NA2APM)]**	31.5	22.3	6.4	5.4	1139	850	1425	1300	0.36±0.01	0.39±0.03	0.40±0.02	0.50±0.02	45.7	42.3
12	**[Eu(DBM)$_3$(NTF2AP)]**	27.1	40.5	5.1	3.0	980	1378	1273	655	0.51±0.07	0.27±0.03	0.52±0.03	0.30±0.02	50.6	40.7
13	**[Eu(DBM)$_3$(NTF2APM)]**	20.0	32.8	15.3	4.4	964	1163	5747	3403	0.07±0.01	0.22±0.01	0.10±0.04	0.29±0.03	9.3	34.2
14	**[Eu(DBM)$_3$(NB2AP)$_2$]**	33.5	31.3	6.6	6.8	1204	1137	2672	1296	0.38±0.01	0.36±0.01	0.47±0.01	0.39±0.04	56.2	44.5
15	**[Eu(DBM)$_3$(NB2APM)]**	26.4	27.7	7.5	6.8	1017	1028	2874	1491	0.27±0.01	0.41±0.01	0.32±0.05	0.43±0.02	32.2	44.3
16	**[Eu(DBM)$_3$(BIPY)]**	27.2	28.6	4.0	4.3	968	1007	1477	1340	0.44±0.01	0.47±0.01	0.50±0.05	0.56±0.05	48.7	56.4
17	**[Eu(TTA)$_3$(H$_2$O)$_2$]**	26.9	27.6	6.3	7.1	980	1018	3525	2873	0.23±0.01	0.26±0.01	0.24±0.01	0.29±0.02	23.3	29.3
18	**[Eu(TTA)$_3$(NA2AP)]**	25.0	22.0	6.0	12.3	928	945	1696	1173	0.38±0.00	0.48±0.00	0.41±0.04	0.52±0.01	37.7	49.5
19	**[Eu(TTA)$_3$(NA2APM)$_2$]**	19.9	22.6	16.1	13.7	978	1013	1110	649	0.44±0.01	0.47±0.00	0.48±0.02	0.57±0.01	47.1	57.8
20	**[Eu(TTA)$_3$(NTF2AP)$_2$]**	14.0	19.4	14.2	10.7	767	837	1416	602	0.45±0.02	0.45±0.02	0.46±0.02	0.48±0.03	35.5	40.2
21	**[Eu(TTA)$_3$(NTF2APM)]**	32.9	29.2	6.1	6.9	1198	1079	1283	654	0.49±0.05	0.49±0.06	0.43±0.04	0.37±0.03	51.5	39.8
22	**[Eu(TTA)$_3$(NB2AP)$_2$]**	16.0	27.6	14.5	8.7	822	1046	1542	970	0.45±0.03	0.48±0.01	0.47±0.04	0.54±0.03	39.9	56.5
23	**[Eu(TTA)$_3$(NB2APM)]**	22.4	22.0	8.8	9.5	881	878	2398	1442	0.38±0.01	0.48±0.01	0.38±0.01	0.52±0.02	33.5	45.6
24	**[Eu(TTA)$_3$(BIPY)]**	17.3	15.8	8.8	6.6	730	649	860	909	0.70±0.01	0.66±0.03	0.64±0.08	0.61±0.10	47.0	39.6

* $\lambda_{exc.}$ = 394 nm

The results show no relationship between the intensity parameters and the fact that one or two amides are coordinated, both for DBM complexes and for TTA complexes. Also, there are no simple relationships such as inductive effects between the different radical groups in the amides used as ancillary ligands and the radiative properties. The great variability in the values of intensity parameters and consequently the radiative rates might be rationalized by taking into account thermally induced changes in the coordination polyhedron of the complexes as it will be discussed in the next section.

3.4 Theoretical evidence of thermally induced changes in the coordination polyhedron

The equilibrium geometries of Eu^{3+} complexes were obtained and used to extract the structure of each ligand. These ligand structures were isolated and the ligand effective polarizability was calculated using the LMOs located at the spatial region defined by two chemical bonds from the Eu^{3+} ion, as defined in Ref [61]. The numerical results for the ligand and Eu–L bonds properties are depicted in Table 2. The first thing that can be observed is that the $\bar{\alpha}_{mol}$ not necessarily follow the same trend of α'. These trends are opposite for the ancillary ligands. When the ancillary ligand changes from xAP to xAPM (x = NA2, NB2, NTF2), the $\bar{\alpha}_{mol}$ decrease while α' increase. The difference from xAP to xAPM is an additional nitrogen atom at the six-membered ring, as it can be seen in Figs. 6d and 6g, for example. This type of structural change induces a modification at the ligand electronic structure, where N atom has a nonbonding electron pair directed out of the ring. However, the xAP to xAPM modification also withdraws a C–H bond, causing the reduction of the molecular polarizability by 0.84 – 0.89 $Å^3$, that is approximately the C–H contribution to the total $\bar{\alpha}_{mol}$. In contrast, the obtained α' values consider the chemical environment localized at the coordination polyhedron and follow a peculiar trend regard the xAP to xAPM differences. It is important to highlight that the photophysical properties observed in this work are not directly dependent on the type of ancillary ligand. In fact, it will be shown that the observed modifications are consequences of the thermal-induced changes in compound geometry. Besides that, the theoretical modeling of the system indicates that the ancillary ligand modification induces changes in coordination polyhedron, modifying the photophysical properties, like the intensity parameters.

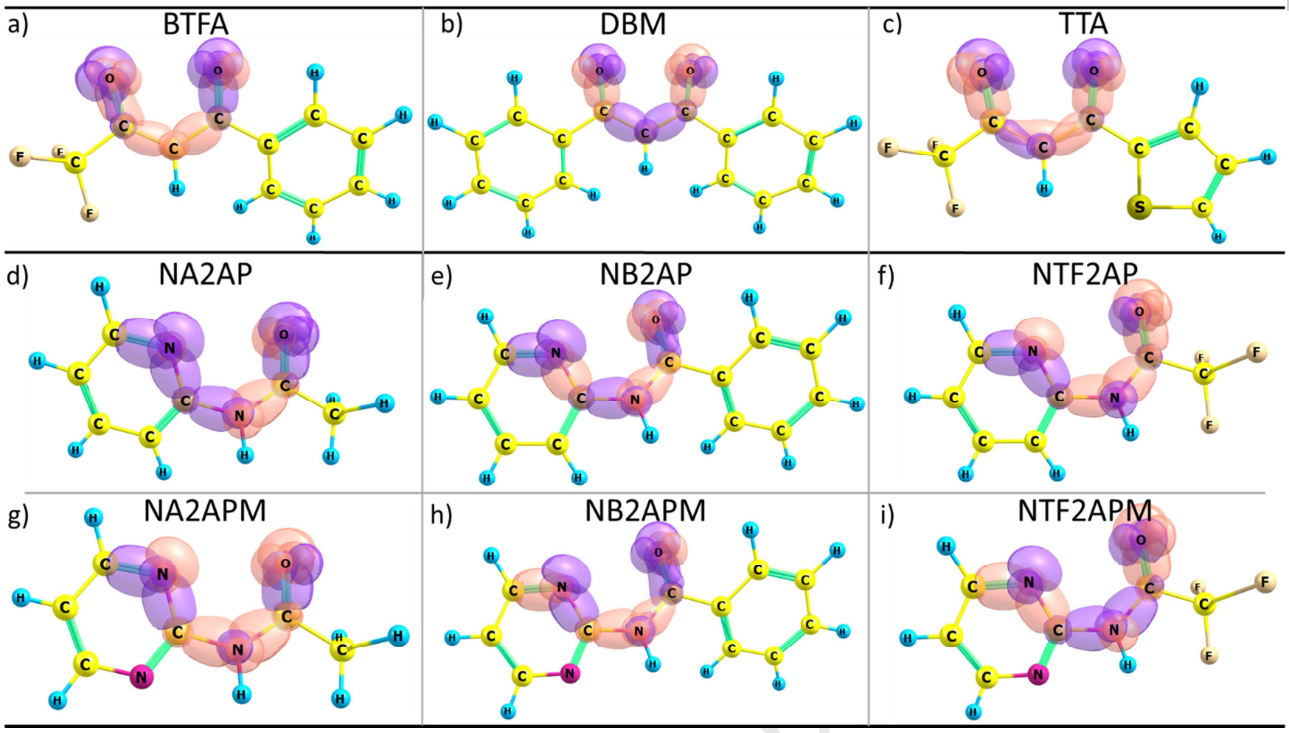

Figure 6. Ligand structures and LMOs superpositions, for the set of studied ligands, used to calculate the ligand effective polarizabilities α'. Isosurfaces generated for 0.2 e/a_0^3.

The α' values for the ligands xAP (NA2AP, NB2AP, and NTF2AP) are close to 2.65 Å^3, not exhibiting a systematic variation. On the other hand, for the pyrimidin ligands, the ligand effective polarizabilities follow the trend: $\alpha'_{\mathrm{NB2APM}} > \alpha'_{\mathrm{NA2APM}} > \alpha'_{\mathrm{NTF2APM}}$. It is thus indicated that the NB2APM together with the DBM (greatest $\alpha'_{\mathrm{DBM}} = 3.38$ Å^3) ligands should effectively grant the most polarizable environment to the Eu^{3+} ion. The same conclusion can be made if the α_{OP} values are analyzed in Table 2. In fact, for this ligand combination, the α_{OP} values are the greatest. Besides that, the α', α_{OP} and g values for the overall ligands are in good agreement with the ones usually obtained for these class of compounds [61].

Although the values of α', α_{OP}, and g are appropriate to calculate the theoretical intensity parameters, they do not provide Ω_λ^{theo} close to Ω_λ^{exp}. This mismatch is probably due to the calculated polyhedron geometries. In fact, for the set of compounds with the same main ligand, the used structural model (DFT calculation in vacuum for molecular units) lead to very similar first coordination spheres, as can be seen at the root mean square deviation (r.m.s.d.) in Tables S3–S5 calculated for all complexes with the same main ligand.

Table 2. Ligand and Eu–L bonds properties for different ligands. Mean molecular isotropic polarizability $\bar{\alpha}_{mol}$ (in Å^3), effective ligand polarizability α'(in Å^3), Eu–L chemical bonds overlap polarizability α_{OP} (in 10^{-2} Å^3) and charge factor g (dimensionless).

	Ligand	$\bar{\alpha}_{mol}$	α'	α_{OP}	g
Main ligands	BTFA	22.46	3.00	3.66	1.44
	DBM	32.70	3.38	3.71	1.45
	TTA	21.71	3.09	3.64	1.44
Ancillary ligands	NA2AP	15.78	2.68	Eu–O: 3.19 Eu–N: 1.06	Eu–O: 1.35 Eu–N: 1.82
	NA2APM	14.94	2.85	Eu–O: 2.99 Eu–N: 1.01	Eu–O: 1.34 Eu–N: 1.82
	NB2AP	24.99	2.62	Eu–O: 2.83 Eu–N: 1.12	Eu–O: 2.00 Eu–N: 2.68
	NB2APM	24.15	2.97	Eu–O: 3.26 Eu–N: 1.06	Eu–O: 1.91 Eu–N: 2.60
	NTF2AP	15.99	2.63	Eu–O: 2.78 Eu–N: 0.91	Eu–O: 1.36 Eu–N: 1.85
	NTF2APM	15.10	2.68	Eu–O: 2.79 Eu–N: 0.95	Eu–O: 1.50 Eu–N: 1.85

It can be observed in Tables S3–S5 that the first coordination sphere for different ancillary ligands (for the same main ligand) are very similar, exhibiting r.m.s.d. less than 0.1 Å. It is important to highlight that any temperature effects (changes from 77 to 300 K) are not considered at the structural model adopted to the obtention of the geometries. So, the JOYSpectra program can be conveniently used in order to access geometry in the first polyhedron geometries induced by temperature effects. In these calculations, three average geometries were used (Table S6), one for each type of complexes with main ligand (BTFA, DBM, and TTA). Then, the distances (only the ancillary groups) and angular deformations (as shown in Fig. 7) were performed and the Ω_λ^{theo} values were recorded. In this way, it is possible to create an outline map of the Ω_λ^{theo} values as a function of the distance and angle, as depicted in Fig. 8. It is important to emphasize that the α', α_{OP} and g values shown in Table 2 were used to construct the graphs in Fig. 8. In Table 3, Figs. 7 and 8, the group distances (GD) and deformation angles (ϕ) are regarded only to the ancillary ligand and the ancillary ligand with one β-dik ligand, respectively.

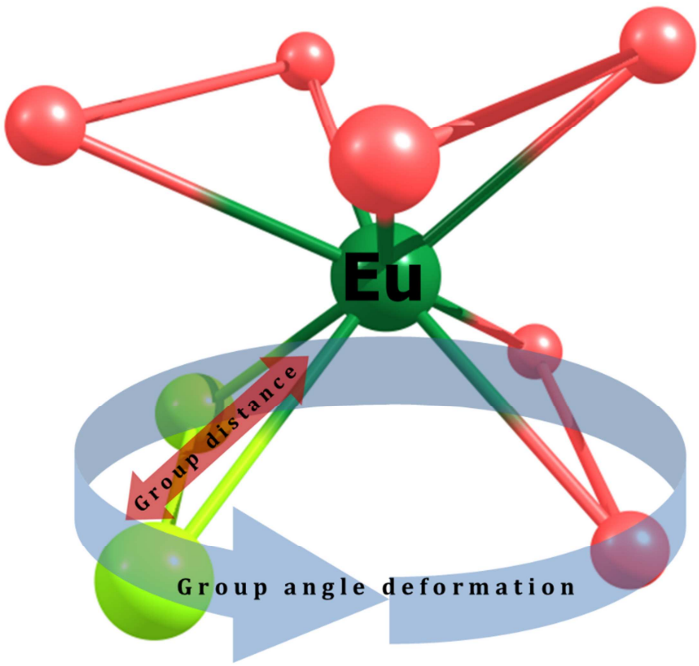

Figure 7. Representation of the structural deformations applied by the JOYSpectra program. The red atoms represent the main ligands while the yellow atoms represent ancillary ligands. The angle deformation is made only in the four atoms at the lower, freezing the upper ligands. The group deformation is made with the approximation/separation of the ancillary ligands.

Table 3. Theoretical intensity parameters Ω_{λ}^{theo} (in 10^{-20} cm^2) of the [Eu(β-dik)$_3$(AL)$_x$] compounds obtained through structural deformations (ϕ angle and ancillary group distances GD in □) simulating the temperature changes (77 and 300 K). AL means ancillary ligands (NA2AP, NA2APM, NTF2AP, NTF2APM, NB2AP, and NB2APM; x = 1 or 2) and β-dik are the main ligands (BTFA, DBM, and TTA).

Entry	Complex	Ω_2^{theo} (10^{-20} cm^2)		Ω_4^{theo} (10^{-20} cm^2)		ϕ (degree)		GD (□)	
		300 K	77 K	300 K	77 K	300 K	77 K	300 K	77 K
1	**[Eu(BTFA)$_3$(H$_2$O)$_2$]**	--	--	--	--				
2	**[Eu(BTFA)$_3$(NA2AP)]**	28.8	24.3	6.1	7.1	4	2	2.55	2.35
3	**[Eu(BTFA)$_3$(NA2APM)]**	22.5	20.7	10.3	5.9	6	68	2.05	2.05
4	**[Eu(BTFA)$_3$(NTF2AP)]**	9.3	17.8	5.7	6.9	287	168	2.25	2.25
5	**[Eu(BTFA)$_3$(NTF2APM)]**	16.6	15.5	6.2	5.3	282	269	2.55	2.55
6	**[Eu(BTFA)$_3$(NB2AP)]**	10.0	11.6	6.2	6.4	283	257	2.30	2.25
7	**[Eu(BTFA)$_3$(NB2APM)]**	10.1	20.5	7.8	6.6	267	192	2.25	2.25
8	**[Eu(BTFA)$_3$(BIPY)]**	--	--	--	--				
9	**[Eu(DBM)$_3$(H$_2$O)]**	--	--	--	--				
10	**[Eu(DBM)$_3$(NA2AP)]**	30.5	33.1	5.8	5.3	292	249	2.50	2.50
11	**[Eu(DBM)$_3$(NA2APM)]**	29.7	23.4	6.0	5.7	70	249	2.30	2.30
12	**[Eu(DBM)$_3$(NTF2AP)]**	29.8	35.1	5.7	2.5	69	35	2.30	2.30
13	**[Eu(DBM)$_3$(NTF2APM)]**	18.9	31.4	13.1	4.2	92	332	2.10	2.10
14	**[Eu(DBM)$_3$(NB2AP)$_2$]**	34.0	34.0	7.1	7.4	75	76	2.4	2.4
15	**[Eu(DBM)$_3$(NB2APM)]**	28.0	29.3	8.0	7.3	107	74	2.30	2.30
16	**[Eu(DBM)$_3$(BIPY)]**	--	--	--	--				
17	**[Eu(TTA)$_3$(H$_2$O)$_2$]**	--	--	--	--				
18	**[Eu(TTA)$_3$(NA2AP)]**	25.4	23.4	6.2	12.9	19	2	2.35	2.05
19	**[Eu(TTA)$_3$(NA2APM)$_2$]**	13.7	23.4	11.0	12.8	103	359	2.05	2.05
20	**[Eu(TTA)$_3$(NTF2AP)$_2$]**	13.8	23.3	12.9	12.7	92	5	2.05	2.05
21	**[Eu(TTA)$_3$(NTF2APM)]**	28.2	28.3	5.2	6.7	77	80	2.55	2.55
22	**[Eu(TTA)$_3$(NB2AP)$_2$]**	14.1	22.2	11.8	6.8	90	340	2.10	2.10
23	**[Eu(TTA)$_3$(NB2APM)]**	22.8	22.4	8.9	9.6	348	12	2.15	2.15
24	**[Eu(TTA)$_3$(BIPY)]**	--	--	--	--				

Once the map has been obtained, different compounds can be pointed out to a pair of group distance and angular deformation (each marker in Fig. 8). In this sense, the geometric variations due to the type of ancillary ligand and thermal effects are accounted to the compound geometry by fitting the Ω_{λ}^{theo} values to Ω_{λ}^{exp} ones.

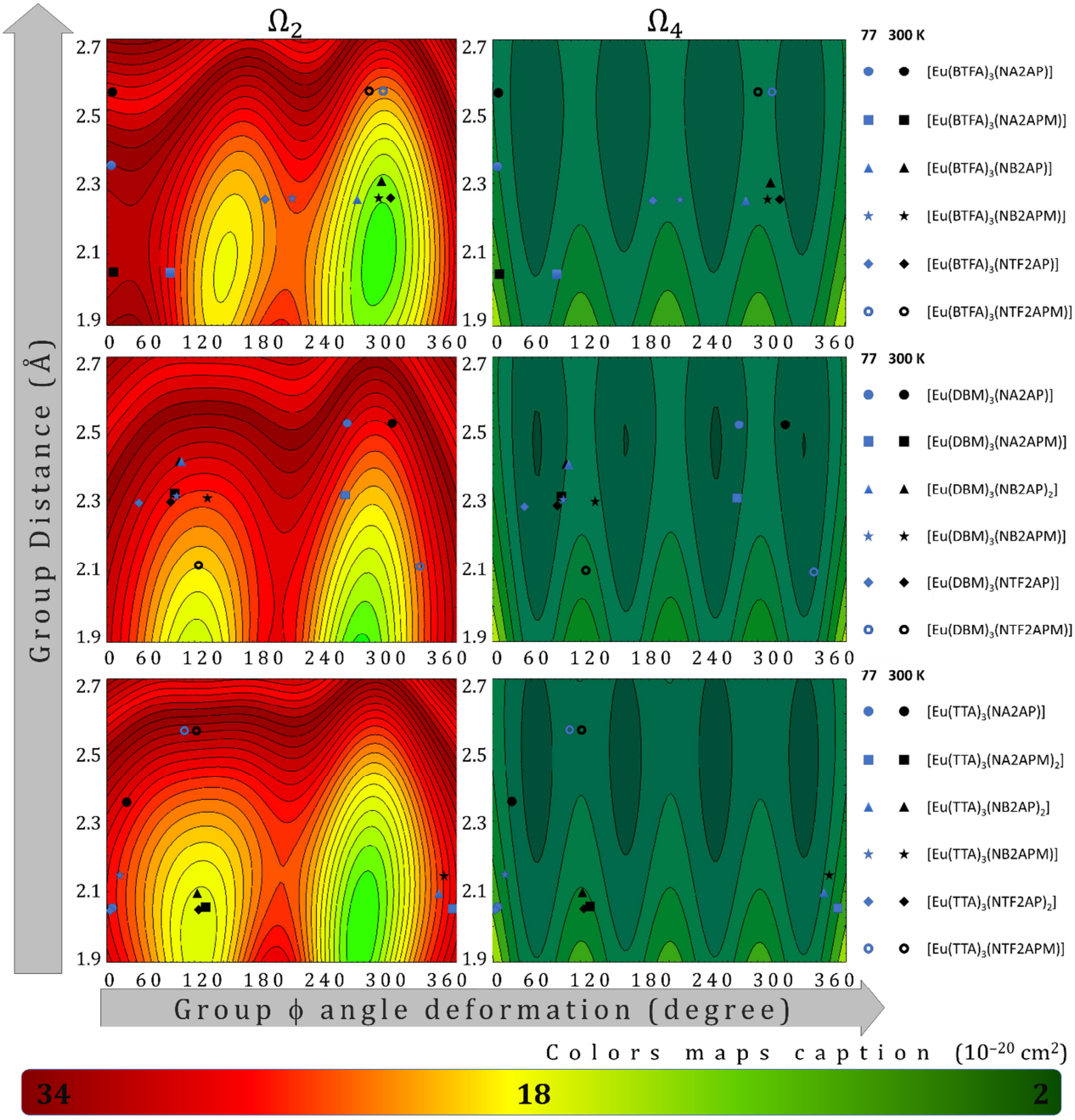

Figure 8. Intensity parameters $\Omega_{\lambda=2,4}$ (10^{-20} cm^2) outline maps as a function of angular deformation ϕ (degree) and ancillary group distance (□) variations for each main ligand (BTFA at the top, DBM in the middle and TTA at the bottom). The different ancillary ligands are represented by different markers for compounds at 77 K (blue color) and 300 K (black color).

Some punctual cases are important to discuss. For example, the [Eu(BTFA)$_3$(NTF2AP)] complex (entry 4 in Table 1) exhibits Q_{Ln}^{Ln} at 77 K almost twice the value at 300 K. This is due to a significant increase in the A_{rad} and even higher decrease in A_{nrad}, both behaviors contributing to the increase of Q_{Ln}^{Ln}. On the other hand, the complexes [Eu(BTFA)$_3$(NA2APM)] and [Eu(DBM)$_3$(NA2APM)] (entries 3 and 11 in Table 1) exhibit values of Q_{Ln}^{Ln} at 77 K lower than at 300 K, which is quite unusual. In these cases, even though both complexes present decrease in A_{nrad} values, they present an even higher decrease in A_{rad} which accounts for the decrease in Q_{Ln}^{Ln}. This behavior might be rationalized by the geometric changes thermally induced which implicate changes in Ω_2 and Ω_4 as shown in Figure 8 and Table 3.

Analyzing the results depicted in Fig. 8 and Table 3, it is possible to observe three trends about the deformations on the coordination polyhedron structures:

1) at low temperatures, when the intensity parameters Ω_4 (77 K) > Ω_4 (300 K) for the same complex, the ancillary ligands are closer (short group distance) to the Eu^{3+} ion. This behavior is explained by the more sensitivity of the Ω_4 to the ligand distance than the Ω_2 parameter, as a consequence of the increase in covalency, quantified directly by the α_{OP} and indirectly by the g values. In other words, the decrease in temperature can change for a more compact structure.

2) The angular variations affect more Ω_2 than Ω_4, being this trend supported when the Ω_2 have a large variation (far away from experimentally determined error) on ϕ ($\Delta\phi = \phi_{300\,K} - \phi_{77\,K} \geq 75°$) (*e.g.* [Eu(BTFA)$_3$NB2APM], [Eu(DBM)$_3$NA2APM], and [Eu(TTA)$_3$(NTF2AP)$_2$] complexes).

3) The complexes without a huge variation in both Ω_2 and Ω_4 present similar variations in ϕ and G.D. (ancillary group distance), as can be noted in [Eu(BTFA)$_3$NTF2APM], [Eu(DBM)$_3$(NB2AP)$_2$], and [Eu(TTA)$_3$NTF2APM] cases.

4. Conclusions

Eighteen new Eu^{3+} complexes and their Gd^{3+} analogues with 1,3-β-diketonate (BTFA, DBM and TTA) as main ligands and N-(pyridine-2-yl)amides (NA2AP, NBF2AP and NTF2AP) or N-(pyrimidine-2-yl)amides (NA2APM, NBF2APM and NTF2APM) as ancillary ligands were synthesized and characterized by elemental analysis, thermogravimetry and infrared spectroscopy. The replacement of water molecules by the pyridil and pyrimidil amides in the Eu^{3+} complexes increased significantly the intrinsic quantum yields of luminescence (Q_{Ln}^{Ln}). In these complexes, geometric variations are attributed to temperature changes and, as a

consequence, variations in the Judd-Ofelt intensity parameters (Ω_2 and Ω_4) for the Eu^{3+} complexes. These variations do not show apparently follow any systematic trends. Geometric modeling (on the azimuthal angle ϕ and ancillary ligands distances) carried out *in silico* experiments corroborates these conclusions. Finally, the joint action of the present ancillary ligand together with the β-diketonates ligands has proven to be quite efficient in improving the luminescence with respect to the usual ancillary BIPY.

Acknowledgments

The authors thank the following Brazilian agencies for financial support: Conselho Nacional de Desenvolvimento Científico e Tecnológico (CNPq), PRONEX-FACEPE-CNPQ, INCT-INEO, and the Coordenação de Aperfeiçoamento de Pessoal de Nível Superior (CAPES). A.N.C.N. thanks to SusPhotoSolutions - Soluções Fotovoltaicas Sustentáveis, CENTRO-01-0145-FEDER-000005.

References

[1] M.E. de Mesquita, G.F. de Sá, O.L. Malta, Spectroscopic studies of the Eu(III) and Gd(III) tris(3-aminopyridine-2-carboxylic acid) complexes, J. Alloys Compd. 250 (1997) 417–421. doi:10.1016/S0925-8388(96)02561-3.

[2] H.. Brito, O.. Malta, J.F.. Menezes, Luminescent properties of diketonates of trivalent europium with dimethyl sulfoxide, J. Alloys Compd. 303–304 (2000) 336–339. doi:10.1016/S0925-8388(00)00604-6.

[3] A. Knyazev, S. Krupin, B. Heinrich, B. Donnio, Y.G. Galyametdinov, Controlled polarized luminescence of smectic lanthanide complexes, Dye. Pigment. 148 (2018) 492–500. doi:10.1016/j.dyepig.2017.08.018.

[4] J. Liu, H.-W. Wu, Low-efficient luminescence of a novel iridium complex: Effect of auxiliary ligand of β-diketone derivative with trifluoromethyl on luminous efficiency, J. Lumin. 192 (2017) 701–706. doi:10.1016/j.jlumin.2017.07.025.

[5] T.A. Kovacs, M.C.F.C. Felinto, T.B. Paolini, B. Ali, L.K.O. Nakamura, E.E.S. Teotonio, H.F. Brito, O.L. Malta, Synthesis and photoluminescence properties of [$Eu(dbm)_3$·PX] and [$Eu(acac)_3$·PX] complexes, J. Lumin. 193 (2018) 98–105. doi:10.1016/j.jlumin.2017.09.029.

[6] L. Zhang, X. Wang, X.-Y. Zhao, The reversible mechanofluorochromic property of an

asymmetric diketonate boron complex at room temperature, J. Lumin. 202 (2018) 420–426. doi:10.1016/j.jlumin.2018.05.073.

[7] S.A. Junior, F.V. de Almeida, G.F. de Sá, C. de Mello Donegá, Luminescence and quantum yields of Eu^{3+} mixed complexes with 1-phenyl-1,3-butanedione and 1,10-phenanthroline or 1,10-phenanthroline-N-oxide, J. Lumin. 72–74 (1997) 478–480. doi:10.1016/S0022-2313(97)00025-2.

[8] C. de Mello Donegá, S.A. Junior, G.. de Sá, Synthesis, luminescence and quantum yields of Eu(III) mixed complexes with 4,4,4-trifluoro-1-phenyl-1,3-butanedione and 1,10-phenanthroline-N-oxide, J. Alloys Compd. 250 (1997) 422–426. doi:10.1016/S0925-8388(96)02562-5.

[9] P. Shukla, V. Sudarsan, R.K. Vatsa, S.K. Nayak, S. Chattopadhyay, Effect of symmetric substitution on the phenyl groups of Eu^{3+}-dibenzoyl methane complexes on their luminescence properties, J. Lumin. 130 (2010) 1952–1957. doi:10.1016/j.jlumin.2010.05.011.

[10] P.P. Lima, M.M. Nolasco, F.A.A. Paz, R.A.S. Ferreira, R.L. Longo, O.L. Malta, L.D. Carlos, Photo-click chemistry to design highly efficient lanthanide β-diketonate complexes stable under UV irradiation, Chem. Mater. 25 (2013) 586–598. doi:10.1021/cm303776x.

[11] A.A. Knyazev, M.E. Karyakin, K.A. Romanova, B. Heinrich, B. Donnio, Y.G. Galyametdinov, Influence of Lewis Bases on the Mesogenic and Luminescent Properties of Homogeneous Films of Europium(III) Tris(β-diketonate) Adducts, Eur. J. Inorg. Chem. 2017 (2017) 639–645. doi:10.1002/ejic.201601286.

[12] E. Niyama, H.F. Brito, M. Cremona, E.E.S. Teotonio, R. Reyes, G.E.S. Brito, M.C.F.C. Felinto, Synthesis and spectroscopic behavior of highly luminescent Eu^{3+}-dibenzoylmethanate (DBM) complexes with sulfoxide ligands, Spectrochim. Acta - Part A Mol. Biomol. Spectrosc. 61 (2005) 2643–2649. doi:10.1016/j.saa.2004.10.006.

[13] E.E.S. Teotonio, G.M. Fett, H.F. Brito, W.M. Faustino, G.F. de Sá, M.C.F.C. Felinto, R.H.A. Santos, Evaluation of intramolecular energy transfer process in the lanthanide(III) bis- and tris-(TTA) complexes: Photoluminescent and triboluminescent behavior, J. Lumin. 128 (2008) 190–198. doi:10.1016/j.jlumin.2007.07.005.

[14] O.L. Malta, H.F. Brito, J.F.S. Menezes, F.R.G.E. Silva, C.D. Donega, S. Alves, Experimental and theoretical emission quantum yield in the compound Eu(thenoyltrifluoroacetonate)3.2(dibenzyl sulfoxide), Chem. Phys. Lett. 282 (1998)

233–238. doi:10.1016/S0009-2614(97)01283-9.

[15] H. Xu, Q. Sun, Z. An, Y. Wei, X. Liu, Electroluminescence from europium(III) complexes, Coord. Chem. Rev. 293–294 (2015) 228–249. doi:10.1016/j.ccr.2015.02.018.

[16] D.B.A. Raj, B. Francis, M.L.P. Reddy, R.R. Butorac, V.M. Lynch, A.H. Cowley, Highly luminescent poly(methyl methacrylate)-incorporated europium complex supported by a carbazole-based fluorinated 4,5-bis(diphenylphosphino)-9,9- dimethylxanthene oxide Co-ligand, Inorg. Chem. 49 (2010) 9055–9063. doi:10.1021/ic1015324.

[17] V. Divya, M.L.P. Reddy, Visible-light excited red emitting luminescent nanocomposites derived from Eu3+-phenathrene-based fluorinated β-diketonate complexes and multi-walled carbon nanotubes, J. Mater. Chem. C. 1 (2013) 160–170. doi:10.1039/c2tc00186a.

[18] G.F. de Sá, O.L. Malta, C. de Mello Donegá, A.M. Simas, R.L. Longo, P.A. Santa-Cruz, E.F. da Silva, Spectroscopic properties and design of highly luminescent lanthanide coordination complexes, Coord. Chem. Rev. 196 (2000) 165–195. doi:10.1016/S0010-8545(99)00054-5.

[19] M. Latva, H. Takalo, V.-M. Mukkala, C. Matachescu, J.C. Rodríguez-Ubis, J. Kankare, Correlation between the lowest triplet state energy level of the ligand and lanthanide(III) luminescence quantum yield, J. Lumin. 75 (1997) 149–169. doi:10.1016/S0022-2313(97)00113-0.

[20] A.S. Souza, L.A. Nunes, M.C.F.C. Felinto, H.F. Brito, O.L. Malta, On the quenching of trivalent terbium luminescence by ligand low lying triplet state energy and the role of the $^7F_5$ level: The $[Tb(tta)_3(H_2O)_2]$ case, J. Lumin. 167 (2015) 167–171. doi:10.1016/j.jlumin.2015.06.020.

[21] H.F. Brito, C.A.A. Carvalho, O.L. Malta, J.J. Passos, J.F.S. Menezes, R.D. Sinisterra, Spectroscopic study of the inclusion compound of β-cyclodextrin and tris(dibenzoylmethane)europium(III) dihydrate, Spectrochim. Acta - Part A Mol. Biomol. Spectrosc. 55 (1999) 2403–2410. doi:10.1016/S1386-1425(99)00034-7.

[22] E.E.S. Teotonio, F.A. Silva, D.K.S. Pereira, L.M. Santo, H.F. Brito, W.M. Faustino, M.C.F.C. Felinto, R.H. Santos, R. Moreno-Fuquen, A.R. Kennedy, D. Gilmore, Luminescence enhancement of the Tb(III) ion with the thenoyltrifluoroacetonate ligand acting as an efficient sensitizer, Inorg. Chem. Commun. 13 (2010) 1391–1395. doi:10.1016/j.inoche.2010.07.043.

[23] D. Chitnis, N.T. Kalyani, S.J. Dhoble, Portrayal of structural, thermal and optical properties of pH sensitive Eu(TTA)$_3$bipy hybrid organic complex for OLEDs, Optik (Stuttg). 130 (2017) 237–244. doi:10.1016/j.ijleo.2016.08.127.

[24] S. Wu, P. He, J. Guan, B. Chen, Y. Luo, Q. Yan, Q. Zhang, Effects of synergetic ligands on structure and fluorescence properties of Langmuir and Langmuir-Blodgett films containing Eu(TTA)$_3$nL, J. Photochem. Photobiol. A Chem. 188 (2007) 218–225. doi:10.1016/j.jphotochem.2006.12.020.

[25] C. Freund, W. Porzio, U. Giovanella, F. Vignali, M. Pasini, S. Destri, A. Mech, S. Di Pietro, L. Di Bari, P. Mineo, Thiophene based europium β-diketonate complexes: Effect of the ligand structure on the emission quantum yield, Inorg. Chem. 50 (2011) 5417–5429. doi:10.1021/ic1021164.

[26] E.R. dos Santos, R.O. Freire, N.B. da Costa, F.A.A. Paz, C.A. de Simone, S.A. Júnior, A.A.S. Araújo, L.A.O. Nunes, M.E. de Mesquita, M.O. Rodrigues, Theoretical and Experimental Spectroscopic Approach of Fluorinated Ln^{3+}–β-Diketonate Complexes, J. Phys. Chem. A. 114 (2010) 7928–7936. doi:10.1021/jp104038r.

[27] H.J. Batista, A.V.M. de Andrade, R.L. Longo, A.M. Simas, G.F. de Sá, N.K. Ito, L.C. Thompson, Synthesis, X-ray Structure, Spectroscopic Characterization, and Theoretical Prediction of the Structure and Electronic Spectrum of Eu(btfa)$_3$·bipy and an Assessment of the Effect of Fluorine as a β-Diketone Substituent on the Ligand−Metal Energy, Inorg. Chem. 37 (1998) 3542–3547. doi:10.1021/ic971602v.

[28] Y.-W. Yip, H. Wen, W.-T. Wong, P.A. Tanner, K.-L. Wong, Increased Antenna Effect of the Lanthanide Complexes by Control of a Number of Terdentate N-Donor Pyridine Ligands, Inorg. Chem. 51 (2012) 7013–7015. doi:10.1021/ic300916e.

[29] A. Bencini, V. Lippolis, 1,10-Phenanthroline: A versatile building block for the construction of ligands for various purposes, Coord. Chem. Rev. 254 (2010) 2096–2180. doi:10.1016/j.ccr.2010.04.008.

[30] G. Sharma, A.K. Narula, Synthesis of Eu(III) complexes with 2-aminopyridine and 1,10-phenanthroline: Structural, optical, thermal and morphological studies, Sensors Actuators, B Chem. 215 (2015) 584–591. doi:10.1016/j.snb.2015.03.102.

[31] H.J. Batista, R.L. Longo, Improved point-charge model within the INDO/S-CI method for describing the ligand excited states of lanthanide coordination compounds, Int. J. Quantum Chem. 90 (2002) 924–932. doi:10.1002/qua.10031.

[32] W.. Faustino, G.. Rocha, F.. Gonçalves e Silva, O.. Malta, G.. de Sá, A.. Simas, Design of ligands to obtain lanthanide ion complexes displaying high quantum efficiencies of luminescence using the sparkle model, J. Mol. Struct. THEOCHEM. 527 (2000) 245–251. doi:10.1016/S0166-1280(00)00497-8.

[33] W.M. Faustino, S.A. Junior, L.C. Thompson, G.F. De Sá, O.L. Malta, A.M. Simas, Theoretical and experimental luminescence quantum yields of coordination compounds of trivalent europium, Int. J. Quantum Chem. 103 (2005) 572–579. doi:10.1002/qua.20582.

[34] N. Filipescu, K. Moorjani, N. McAvoy, S. Bjorklund, C.R. Hurt, J. Zumoff, Fluorescence Spectra of Homogeneous and Mixed Europium Complexes, Appl. Spectrosc. 22 (1968) 513–519. doi:10.1366/000370268774384272.

[35] V.A.F. Deichmann, J.B.M. Novo, A. Cirpan, F.E. Karasz, L. Akcelrud, Photo- and Electroluminescent behavior of Eu^{3+} Ions in Blends with poly(vinyl-carbazole), J. Braz. Chem. Soc. 18 (2007) 330–336. doi:10.1590/S0103-50532007000200013.

[36] H.Y. Wong, W.S. Lo, W.T.K. Chan, G.L. Law, Mechanistic Investigation of Inducing Triboluminescence in Lanthanide(III) β-Diketonate Complexes, Inorg. Chem. 56 (2017) 5135–5140. doi:10.1021/acs.inorgchem.7b00273.

[37] T. Ishimoto, Y. Ito, T. Tada, R. Oike, T. Nakamura, K. Amezawa, M. Koyama, Theoretical study on temperature effect of electronic structure and spin state in $LaCoO_3$ by using density functional theory, Solid State Ionics. 285 (2016) 195–201. doi:10.1016/j.ssi.2015.08.017.

[38] A. Jaoul, G. Nocton, C. Clavaguéra, Assessment of Density Functionals for Computing Thermodynamic Properties of Lanthanide Complexes, ChemPhysChem. 18 (2017) 2688–2696. doi:10.1002/cphc.201700629.

[39] G. Nocton, W.W. Lukens, C.H. Booth, S.S. Rozenel, S.A. Medling, L. Maron, R.A. Andersen, Reversible Sigma C–C Bond Formation Between Phenanthroline Ligands Activated by $(C_5Me_5)_2Yb$, J. Am. Chem. Soc. 136 (2014) 8626–8641. doi:10.1021/ja502271q.

[40] A.N. Carneiro Neto, R.T. Moura, O.L. Malta, On the mechanisms of non-radiative energy transfer between lanthanide ions: centrosymmetric systems, J. Lumin. 210 (2019) 342–347. doi:10.1016/j.jlumin.2019.02.049.

[41] A. Shyichuk, R.T. Moura, A.N. Carneiro Neto, M. Runowski, M.S. Zarad, A. Szczeszak, S. Lis, O.L. Malta, Effects of dopant addition on lattice and luminescence intensity parameters of Eu(III)-doped lanthanum orthovanadate, J. Phys. Chem. C. 120 (2016)

28497–28508. doi:10.1021/acs.jpcc.6b10778.

[42] T. Grzyb, A. Szczeszak, A. Shyichuk, R.T. Moura Jr., A.N. Carneiro Neto, N. Andrzejewska, O.L. Malta, S. Lis, Comparative studies of structure, spectroscopic properties and intensity parameters of tetragonal rare earth vanadate nanophosphors doped with Eu(III), J. Alloys Compd. 741 (2018) 459–472. doi:10.1016/j.jallcom.2018.01.095.

[43] M. Nonoyama, S. Tomita, K. Yamasaki, N-(2-Pyridyl)acetamide complexes of palladium(II), cobalt(II), nickel(II), and copper(II), Inorganica Chim. Acta. 12 (1975) 33–37. doi:10.1016/S0020-1693(00)89832-1.

[44] C.A. Faler, M.M. Joullié, Aminolysis of allyl esters with bislithium aryl amides, Tetrahedron Lett. 47 (2006) 7229–7231. doi:10.1016/j.tetlet.2006.07.136.

[45] R.G. Charles, R.C. Ohlmann, Europium thenoyltrifluoroacetonate, preparation and fluorescence properties, J. Inorg. Nucl. Chem. 27 (1965) 255–259. doi:10.1016/0022-1902(65)80222-6.

[46] Y. Luo, B. Chen, W. Wu, X. Yu, Q. Yan, Q. Zhang, Judd-Ofelt treatment on luminescence of europium complexes with β-diketone and bis(β-diketone), J. Lumin. 129 (2009) 1309–1313. doi:10.1016/j.jlumin.2009.06.016.

[47] H.F. Brito, O.M.L. Malta, M.C.F.C. Felinto, E.E.S. Teotonio, Luminescence Phenomena Involving Metal Enolates, in: PATAI'S Chem. Funct. Groups, John Wiley & Sons, Ltd, Chichester, UK, 2010. doi:10.1002/9780470682531.pat0419.

[48] O.L. Malta, L.D. Carlos, Intensities of 4f-4f transitions in glass materials, Quim. Nova. 26 (2003) 889–895. doi:10.1590/S0100-40422003000600018.

[49] I.P. Assunção, A.N. Carneiro Neto, R.T. Moura, C.C.S. Pedroso, I.G.N. Silva, M.C.F.C. Felinto, E.E.S. Teotonio, O.L. Malta, H.F. Brito, Odd-Even Effect on Luminescence Properties of Europium Aliphatic Dicarboxylate Complexes, ChemPhysChem. 20 (2019) 1931–1940. doi:10.1002/cphc.201900603.

[50] W.T. Carnall, H. Crosswhite, H.M. Crosswhite, Energy level structure and transition probabilities in the spectra of the trivalent lanthanides in LaF_3, Argonne, IL (United States), 1978. doi:10.2172/6417825.

[51] B.R. Judd, Optical absorption intensities of rare-earth ions, Phys. Rev. 127 (1962) 750–761. doi:10.1103/PhysRev.127.750.

[52] G.S. Ofelt, Intensities of Crystal Spectra of Rare-Earth Ions, J. Chem. Phys. 37 (1962) 511–520. doi:10.1063/1.1701366.

[53] C.K. Jørgensen, B.R. Judd, Hypersensitive pseudoquadrupole transitions in lanthanides, Mol. Phys. 8 (1964) 281–290. doi:10.1080/00268976400100321.

[54] S.F. Mason, R.D. Peacock, B. Stewart, Ligand-polarization contributions to the intensity of hypersensitive trivalent lanthanide transitions, Mol. Phys. 30 (1975) 1829–1841.

[55] B.R. Judd, Ionic transitions hypersensitive to environment, J. Chem. Phys. 70 (1979) 4830. doi:10.1063/1.437372.

[56] O.L. Malta, Theoretical crystal-field parameters for the YOCl:Eu^{3+} system. A simple overlap model, Chem. Phys. Lett. 88 (1982) 353–356. doi:10.1016/0009-2614(82)87103-0.

[57] O.L. Malta, A simple overlap model in lanthanide crystal-field theory, Chem. Phys. Lett. 87 (1982) 27–29. doi:10.1016/0009-2614(82)83546-X.

[58] R.T. Moura Jr, A.N. Carneiro Neto, R.L. Longo, O.L. Malta, On the calculation and interpretation of covalency in the intensity parameters of 4f–4f transitions in Eu^{3+} complexes based on the chemical bond overlap polarizability, J. Lumin. 170 (2016) 420–430. doi:10.1016/j.jlumin.2015.08.016.

[59] H.B. Bebb, A. Gold, Multiphoton ionization of hydrogen and rare-gas atoms, Phys. Rev. 143 (1966) 1–24. doi:10.1103/PhysRev.143.1.

[60] O.L. Malta, E.A. Gouveia, Comment on the average energy denominator method in perturbation theory, Phys. Lett. A. 97 (1983) 333–334. doi:10.1016/0375-9601(83)90655-2.

[61] R.T. Moura, A.N. Carneiro Neto, R.L. Longo, O.L. Malta, On the calculation and interpretation of covalency in the intensity parameters of 4f-4f transitions in Eu3+ complexes based on the chemical bond overlap polarizability, J. Lumin. 170 (2016) 420–430. doi:10.1016/j.jlumin.2015.08.016.

[62] A.N. Carneiro Neto, R.T. Moura, E.C. Aguiar, C. V Santos, M.A.F.L.B. de Medeiros, Theoretical study of geometric and spectroscopic properties of Eu(III) complexes with Ruhemann's Purple ligands, J. Lumin. 201 (2018) 451–459. doi:10.1016/j.jlumin.2018.05.014.

[63] R.T. Moura, O.L. Malta, R.L. Longo, The chemical bond overlap plasmon as a tool for quantifying covalency in solid state materials and its applications to spectroscopy, Int. J. Quantum Chem. 111 (2011) 1626–1638. doi:10.1002/qua.22782.

[64] M. Abramowitz, I.A. Stegun, Handbook of Mathematical Functions with Formulas,

Graphs, and Mathematical Tables, Dover Publications, 1970.

[65] M.J. Frisch, G.W. Trucks, H.B. Schlegel, G.E. Scuseria, M.A. Robb, J.R. Cheeseman, G. Scalmani, V. Barone, B. Mennucci, G.A. Petersson, H. Nakatsuji, M. Caricato, X. Li, H.P. Hratchian, A.F. Izmaylov, J. Bloino, G. Zheng, J.L. Sonnenberg, M. Hada, M. Ehara, K. Toyota, R. Fukuda, J. Hasegawa, M. Ishida, T. Nakajima, Y. Honda, O. Kitao, H. Nakai, T. Vreven, J.A. Montgomery, J.E. Peralta Jr., F. Ogliaro, M. Bearpark, J.J. Heyd, E. Brothers, K.N. Kudin, V.N. Staroverov, T. Keith, R. Kobayashi, J. Normand, K. Raghavachari, A. Rendell, J.C. Burant, S.S. Iyengar, J. Tomasi, M. Cossi, N. Rega, J.M. Millam, M. Klene, J.E. Knox, J.B. Cross, V. Bakken, C. Adamo, J. Jaramillo, R. Gomperts, R.E. Stratmann, O. Yazyev, A.J. Austin, R. Cammi, C. Pomelli, J.W. Ochterski, R.L. Martin, K. Morokuma, V.G. Zakrzewski, G.A. Voth, P. Salvador, J.J. Dannenberg, S. Dapprich, A.D. Daniels, O. Farkas, J.B. Foresman, J. V. Ortiz, J. Cioslowski, D.J. Fox, Gaussian 09, Revision C.01, (2010).

[66] J.J.P. Stewart, MOPAC2016, (2016). http::://openmopac.net.

[67] J. Pipek, P.G. Mezey, A fast intrinsic localization procedure applicable for ab initio and semiempirical linear combination of atomic orbital wave functions, J. Chem. Phys. 90 (1989) 4916–4926. doi:10.1063/1.456588.

[68] M.W. Schmidt, K.K. Baldridge, J.A. Boatz, S.T. Elbert, M.S. Gordon, J.H. Jensen, S. Koseki, N. Matsunaga, K.A. Nguyen, S. Su, T.L. Windus, M. Dupuis, J.A. Montgomery Jr, General atomic and molecular electronic structure system, J. Comput. Chem. 14 (1993) 1347–1363. doi:10.1002/jcc.540141112.

[69] M. Dolg, H. Stoll, H. Preuss, Energy-adjusted ab initio pseudopotentials for the rare earth elements, J. Chem. Phys. 90 (1989) 1730. doi:10.1063/1.456066.

[70] J.J.P. Stewart, Optimization of parameters for semiempirical methods I. Method, J. Comput. Chem. 10 (1989) 209–220. doi:10.1002/jcc.540100208.

[71] R.O. Freire, G.B. Rocha, A.M. Simas, Sparkle/PM3 for the modeling of europium(III), gadolinium(III), and terbium(III) complexes, J. Braz. Chem. Soc. 20 (2009) 1638–1645. doi:10.1590/S0103-50532009000900011.

[72] G. te Velde, F.M. Bickelhaupt, E.J. Baerends, C. Fonseca Guerra, S.J.A. van Gisbergen, J.G. Snijders, T. Ziegler, Chemistry with ADF, J. Comput. Chem. 22 (2001) 931–967. doi:10.1002/jcc.1056.

[73] E.E.S. Teotonio, H.F. Brito, M.C.F.C. Felinto, C.A. Kodaira, O.L. Malta, Luminescence Investigations on Eu(III) Thenoyltrifluoroacetonate Complexes with Amide Ligands, J.

Coord. Chem. 56 (2003) 913–921. doi:10.1080/0095897031000135333.

[74] K. Nakamoto, Infrared and Raman Spectra of Inorganic and Coordination Compounds, John Wiley & Sons, Inc., Hoboken, NJ, USA, 2008. doi:10.1002/9780470405888.

[75] K. Binnemans, Interpretation of europium(III) spectra, Coord. Chem. Rev. 295 (2015) 1–45. doi:10.1016/j.ccr.2015.02.015.

[76] F.P. Aguiar, I.F. Costa, J.G.P. Espínola, W.M. Faustino, J.L. Moura, H.F. Brito, T.B. Paolini, M.C.F.C. Felinto, E.E.S. Teotonio, Luminescent hybrid materials functionalized with lanthanide ethylenodiaminotetraacetate complexes containing β-diketonate as antenna ligands, J. Lumin. 170 (2016) 538–546. doi:10.1016/j.jlumin.2015.06.038.

Highlights

- New Eu^{3+} diketonates with N-(pyridine-2-yl)amides and .N-(pyrimidine-2-yl)amides.
- New complexes presenting high intrinsic quantum yields of luminescence.
- Experimental and theoretical evidences of thermally induced structural changes.

Conflict of interest: none.